2 Principles of Ionization and Ion Dissociation

Learning Objectives

- Ionization process and ionization energy
- Internal energy of ions and internal energy distribution
- Energetic considerations governing the fragmentation of excited ions
- Quasi-equilibrium theory and rates of unimolecular dissociations
- Time scale of mass spectrometry
- Selected tools of gas phase ion chemistry

The mass spectrometer can be regarded as a kind of chemical laboratory, especially designed to study ions in the gas phase [1,2]. In addition to the task it is commonly used for – creation of mass spectra for a generally analytical purpose – it allows for the examination of fragmentation pathways of selected ions, for the study of ion–neutral reactions and more. Understanding these fundamentals is prerequisite for the proper application of mass spectrometry with all technical facets available, and for the successful interpretation of mass spectra because "analytical chemistry is the application of physical chemistry to the real world" [3].

In the first place, this chapter deals with the fundamentals of gas phase ion chemistry, i.e., with ionization, excitation, ion thermochemistry, ion lifetimes, and reaction rates of ion dissociation. The final sections are devoted to more practical aspects of gas phase ion chemistry such as the determination of ionization and appearance energies or of gas phase basicities and proton affinities.

Brief discussions of some topics of this chapter may also be found in physical chemistry textbooks; however, much better introductions are given in the specialized literature [4-11]. Detailed compound-specific fragmentation mechanisms, ion–molecule complexes, and more are dealt with later (Chap. 6).

2.1 Gas Phase Ionization by Energetic Electrons

Besides some rare experimental setups the mass analyzer of any mass spectrometer can only handle charged species, i.e., ions that have been created from atoms or molecules, occasionally also from radicals, zwitterions or clusters. It is the task of the ion source to perform this crucial step and there is a wide range of ionization methods in use to achieve this goal for the whole variety of analytes.

J. Gross, *Mass Spectrometry*, 2nd ed., DOI 10.1007/978-3-642-10711-5_2,

The classical procedure of ionization involves shooting energetic electrons on a gaseous neutral. This is called *electron ionization* (EI). Electron ionization has formerly been termed *electron impact ionization* or simply *electron impact* (EI). For EI, the neutral previously must have been transferred into the highly diluted gas phase, which is done by means of any sample inlet system suitable for the evaporation of the respective compound. In practice, the gas phase may be regarded highly diluted when the mean free path for the particles becomes long enough to make bimolecular interactions almost impossible within the lifetime of the particles concerned. This is easily achieved at pressures in the range of 10^{-4} Pa usually realized in electron ionization ion sources. Here, the description of EI is restricted to what is essential for an understanding of the ionization process as such [12,13] and the consequences for the fate of the freshly created ions.

2.1.1 Formation of Ions

When a neutral is hit by an energetic electron carrying several tens of electronvolts (eV) of kinetic energy, some of the energy of the electron is transferred to the neutral. If the electron, in terms of energy transfer, collides very effectively with the neutral, the energy transferred can exceed the *ionization energy* (*IE*) of the neutral. Then – from the mass spectrometric point of view – the most desirable process can occur: ionization by ejection of one electron generating a *molecular ion*, a positive *radical ion*:

$$M + e^- \rightarrow M^{+\bullet} + 2e^- \tag{2.1}$$

Depending on the analyte and on the energy of the primary electrons, doubly charged and even triply charged ions may be observed

$$M + e^- \rightarrow M^{2+} + 3e^- \tag{2.2}$$

$$M + e^- \rightarrow M^{3+\bullet} + 4e^- \tag{2.3}$$

While the doubly charged ion, M^{2+}, is an *even-electron ion*, the triply charged ion, $M^{3+\bullet}$, again is an *odd-electron ion*. In addition, there are several other events possible from the electron–neutral interaction, e.g., a less effective interaction will bring the neutral into an electronically excited state without ionizing it.

Examples: EI predominantly creates singly charged ions from the precursor neutral. If the neutral was a molecule as in most cases, it started as having an even number of electrons, i.e., it was an *even-electron* (*closed-shell*) *molecule*. The molecular ion formed must then be a radical cation or an *odd-electron* (*open-shell*) *ion* as these species are termed. For methane we obtain:

$$CH_4 + e^- \rightarrow CH_4^{+\bullet} + 2e^- \tag{2.4}$$

In the rare case the neutral was a radical, the ion created by electron ionization would be even-electron, e.g., for nitric oxide:

$$NO^{\bullet} + e^- \rightarrow NO^+ + 2e^- \tag{2.5}$$

Example: The EI mass spectrum of a phenanthroperylene derivative shows a series of comparatively intensive doubly-charged ions, the one at *m/z* 178 being the doubly-charged molecular ion, the others representing doubly-charged fragment ions (Fig. 2.1) [14]. The occurrence of doubly-charged ions of moderate abundance is quite common in the mass spectra of polycyclic aromatic hydrocarbons (PAHs). For another example of multiply-charged ions in EI spectra cf. Chap. 3.5, for the LDI spectrum of this compound cf. Chap. 11.4.

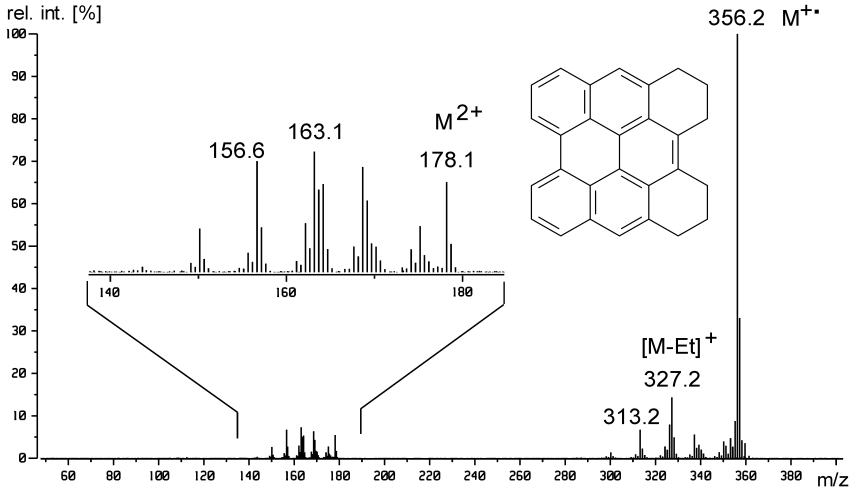

Fig. 2.1. EI mass spectrum of 1,2,3,4,5,6-hexahydrophenanthro[1,10,9,8-*opqra*]perylene. All signals in the expanded inset correspond to doubly-charged ions. Adapted from Ref. [14] with permission. © Elsevier Science, 2002.

2.1.2 Processes Accompanying Electron Ionization

In addition to the desired generation of molecular ions, several other events can result from electron-neutral interactions (Fig. 2.2). A less effective interaction brings the neutral into an electronically excited state without ionizing it. As the energy of the primary electrons increases, the abundance and variety of the ionized species will also increase, i.e., electron ionization may occur via different channels, each of which gives rise to characteristic ionized and neutral products. This includes the production of the following type of ions: molecular ions, fragment ions, multiply charged ions, metastable ions, rearrangement ions, and ion pairs [12].

The electron could also be captured by the neutral to form a negative radical ion. However, *electron capture* (EC) is rather unlikely to occur with electrons of 70 eV since EC is a resonance process because no electron is produced to carry away the excess energy [16]. Thus, EC only proceeds effectively with electrons of very low energy, preferably with thermal electrons (Chap. 7.4). Nonetheless,

molecules containing strongly electronegative elements may form negative ions with low effectivity.

Exceptions: The generation of negative ions from tungsten hexafluoride, WF_6, has been studied under conventional EI conditions. At higher electron energies, $WF_6^{-\bullet}$, WF_5^-, and F^- ions have been found [17]. Organic analytes such as perfluorokerosene also yield negative ions, but sensitivity is lower by some orders of magnitude than for positive-ion EI.

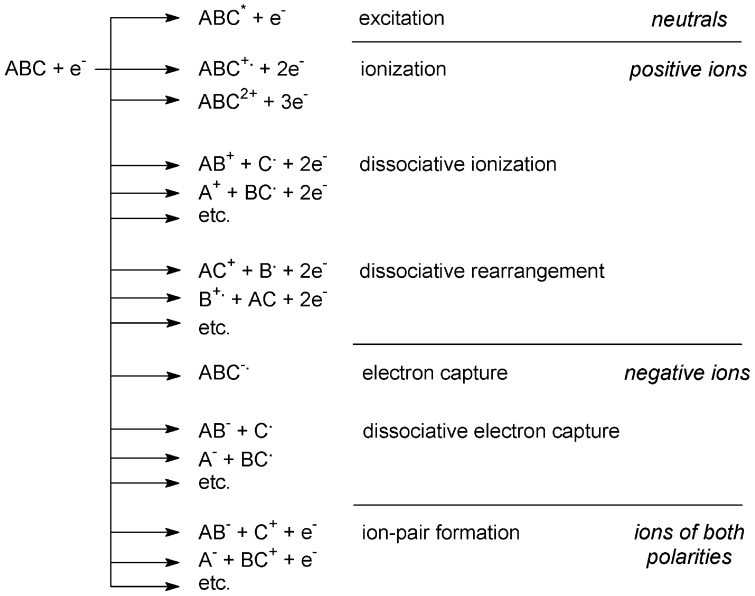

Fig. 2.2. Processes under electron ionization conditions. Under certain conditions, Penning ionization could also play a role. Adapted from Ref. [15] with permission. © Springer-Verlag Heidelberg, 1991.

2.1.3 Ions Generated by Penning Ionization

Non-ionizing electron–neutral interactions create electronically excited neutrals. The ionization reactions occurring when electronically excited neutrals like noble gas atoms, A*, collide with a ground state molecule, M, can be divided into two classes [18]. The first process is *Penning ionization* (Eq. 2.6) [19], the second is *associative ionization*, also known as the *Hornbeck-Molnar process* (Eq. 2.7) [20].

$$A^* + M \rightarrow A + M^{+\bullet} + e^- \tag{2.6}$$

$$A^* + M \rightarrow AM^{+\bullet} + e^- \tag{2.7}$$

Penning ionization occurs with the (trace) gas M having an ionization energy lower than the energy of the metastable state of the excited (noble gas) atoms A*. The above ionization processes have also been employed to construct ion sources [18,21], but until the advent of *direct analysis in real time* (DART, Chap. 13.5), Penning ionization sources were not widely used in analytics.

2.1.4 Ionization Energy

It is obvious that ionization of the neutral can only occur when the energy deposited by the electron-neutral collision is equal to or greater than the *ionization energy* (*IE*) of the corresponding neutral. Formerly, ionization energy has erroneously been termed *ionization potential* (*IP*), as derived from the technique for its experimental determination (Chap. 2.10)..

Definition: The *ionization energy* (*IE*) is defined as the minimum amount of energy that needs to be absorbed by an atom or molecule in its electronic and vibrational ground states in order to form an ion that is also in its ground states by ejection of an electron.

Lone pairs are good sources of an ejectable electron, thus the *IE* of ethanol and dimethylether is lower than that of ethane. It has been shown that the *IE* of a polysubstituted alkane is in principle equal to the *IE* of a structurally otherwise identical monosubstituted alkane bearing the sort of heteroatom which is energetically least demanding for electron loss [22]. The other substituent, provided it is separated by at least two carbon atoms, exerts a very small effect upon the IE. For example, the *IE* of dimethylsulfide, CH_3SCH_3, 8.7 eV, almost equals that of the larger methionine, $CH_3SCH_2CH_2CH(NH_2)COOH$. Introduction of an oxygen decreases the *IE* to a lesser extent than nitrogen, sulfur or even selenium, since these elements have lower electronegativities and thus, are even better sources of the ejected electron. The bottom line of *IE*s is reached when π-systems and heteroatoms are combined in the same molecule.

Note: Ionization energies of most molecules are in the range of 7–15 eV.

2.1.5 Ionization Energy and Charge-Localization

Removal of an electron from a molecule can formally be considered to occur at a σ-bond, a π-bond, or at a lone electron pair with the σ-bond being the least favored and the lone electron pair being the most favored position for *charge-localization* within the molecule, an assumption directly reflected in the *IE*s (Table 2.1). Nobel gases do exist as atoms having closed electron shells and therefore, they exhibit the highest *IE*s. They are followed by diatomic molecules with fluorine, nitrogen, and hydrogen at the upper limit. The *IE* of methane is lower than

Table 2.1. Ionization energies of selected compounds[a]

Compound	IE[b] [eV]	Compound	IE[b] [eV]
Hydrogen, H_2	15.4	Helium, He	24.6
Methane, CH_4	12.6	Neon, Ne	21.6
Ethane, C_2H_6	11.5	Argon, Ar	15.8
Propane, *n*-C_3H_8	10.9	Krypton, Kr	14.0
Butane, *n*-C_4H_{10}	10.5	Xenon, Xe	12.1
Pentane, *n*-C_5H_{12}	10.3		
Hexane, *n*-C_6H_{14}	10.1	Nitrogen, N_2	15.6
Decane, *n*-$C_{10}H_{22}$	9.7	Oxygen, O_2	12.1
		Carbon monoxide, CO	14.0
Ethene, C_2H_4	10.5	Carbon dioxide, CO_2	13.8
Propene, C_3H_6	9.7		
(*E*)-2-Butene, C_4H_8	9.1	Fluorine, F_2	15.7
		Chlorine, Cl_2	11.5
Benzene, C_6H_6	9.2	Bromine, Br_2	10.5
Toluene, C_6H_8	8.8	Iodine, I_2	9.3
Indene, C_9H_8	8.6		
Naphthalene, $C_{10}H_8$	8.1	Ethanol, C_2H_6O	10.5
Biphenyl, $C_{12}H_{10}$	8.2	Dimethylether, C_2H_6O	10.0
Anthracene, $C_{14}H_{10}$	7.4	Ethanethiol, C_2H_6S	9.3
Aniline, C_6H_7N	7.7	Dimethylsulfide, C_2H_6S	8.7
Triphenylamine, $C_{18}H_{15}N$	6.8	Dimethylamine, C_2H_7N	8.2

[a] *IE* data taken from Ref. [23] with permission. © NIST 2002.
[b] All values have been rounded to the first digit.

that of molecular hydrogen but still higher than that of ethane and so forth until the *IE* of long-chain alkanes approaches a lower limit [24]. The more atoms are contained within a molecule the easier it finds a way for stabilization of the charge, e.g., by delocalization or hyperconjugation. Molecules with π-bonds have lower IEs than those without, causing the *IE* of ethene to be lower than that of ethane. Again the *IE* is reduced further with increasing size of the alkene. Aromatic hydrocarbons can stabilize a single charge even better and expanding π-systems also help making ionization easier.

Once the molecular ion is formed, the electron charge is never really localized in a single orbital, although assuming so is often a good working hypothesis for mass spectral interpretation [25,26]. Nonetheless, the concept of charge localization is contradictory to electronegativity that dictates the positive center of an ion should not reside on the more electronegative atom [27]. In case of the molecular ion of pyrrole only 5% of the positive charge reside on the nitrogen, while the adjacent two carbons take about 20% each, and the five hydrogens compensate for the remainder by almost equally contributing ~10% each [27]. Whatever species, it turns out that the charge is delocalized over the whole molecular ion [28-30].

Example: For the *para*-tolyl ion only ~36% of the electron charge rests at the *para*-carbon atom (Fig. 2.3) [31]. In addition, the ionic geometry loses the symmetry of the corresponding neutral molecule.

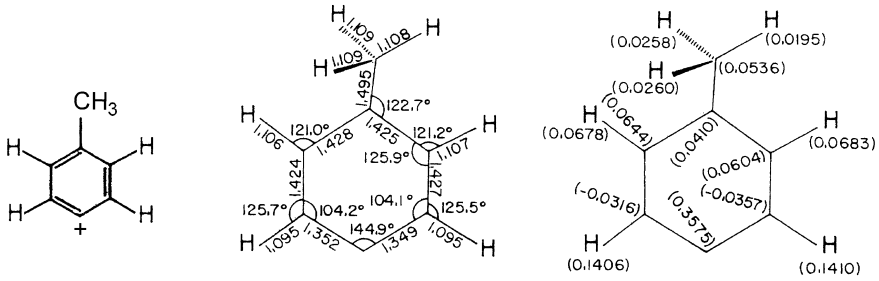

Fig. 2.3. *para*-Tolyl ion, $[C_7H_7]^+$: structural formula (*left*), calculated geometries (*center*) and calculated distributions of formal charge (*right*). Reproduced from Ref. [31] with permission. © American Chemical Society, 1977.

2.2 Vertical Transitions

Electron ionization occurs extremely fast. The time needed for an electron of 70 eV to travel 1 nm through a molecule, a distance roughly corresponding to half a dozen bond lengths, is only about 2×10^{-16} s, and even larger molecules can be traversed in the low femtosecond range. The molecule being hit by the electron can be considered to be at rest because the thermal velocity of a few 100 m s^{-1} is negligible compared to the speed of the electron rushing through. Vibrational motions are slower by at least two orders of magnitude, e.g., even the fast C–H stretching vibration takes 1.1×10^{-14} s per cycle as can be calculated from its IR absorbance at around 3000 cm^{-1}.

According to the *Born-Oppenheimer approximation*, electronic motions and nuclear motions can be separated due to the large mass difference between nuclei and electrons [32-34]. Furthermore, the *Franck-Condon principle* states that electronic transitions will occur on a much faster timescale than it takes the nuclei to move to their new equilibrium positions [34-36]. Applied to the interaction of an energetic electron with a gaseous molecule this means that the positions of the atoms and thus bond lengths remain unaltered during ionization. In diagrams where energy is plotted on the ordinate and bond length on the abscissa, such transitions are represented as *vertical transitions* (Fig. 2.4).

The probability of a particular transition from the ground state neutral to a certain vibrational level of the ion is expressed by its *Franck-Condon factor*. The Franck-Condon factors originate from the fact that the probability for a transition is highest where the electronic wave functions of both ground state and excited state have maximum overlap. While for the ground state this is at equilibrium po-

sition, the wave functions of higher vibrational states have their maxima at the turning points of the motion.

No matter where the electron has formally been taken from, ionization tends to cause weakening of the bonding within the ion as compared to the precursor neutral. Weaker bonding means longer bond lengths on the average and this goes with a higher tendency toward dissociation of a bond. In terms of potential energy surfaces, the situation can easiest be visualized by focusing on just one bond within the molecule or simply by discussing a diatomic molecule. A diatomic molecule has only one vibrational motion, its bond stretching vibration, and therefore its potential energy can be represented by potential energy curves rather than potential energy surfaces. The minimum of the potential energy curve of the neutral, which is assumed to be in its vibrational ground state, is located at shorter bond length, r_0, than the minimum of the radical ion in its ground state, r_1 (Fig. 2.4). Consequently, ionization is accompanied by vibrational excitation because the transitions are vertical, i.e., because the positions of the atoms are actually fixed during this short period.

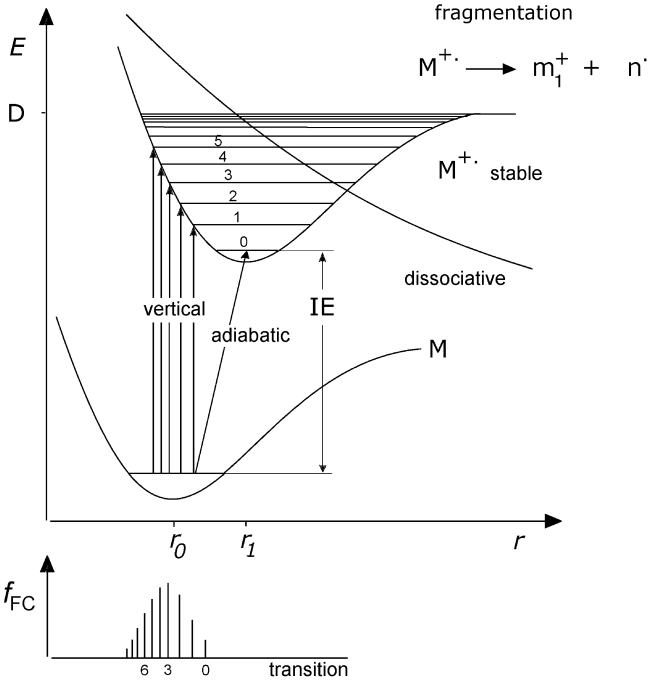

Fig. 2.4. Illustration of the transitions from the neutral to the ionic state for a diatomic molecule. Electron ionization can be represented by a vertical line in this diagram. Thus, ions are formed in a vibrationally excited state if the internuclear distance of the ionic state, r_1, is longer than in the ground state, r_0. Ions having internal energies below the dissociation energy D remain stable, whereas fragmentation will occur above. In few cases, ions are unstable, i.e., there is no minimum on their potential energy curve. The lower part schematically shows the distribution of Franck-Condon factors, f_{FC}, for various transitions.

The distribution of Franck-Condon factors, f_{FC}, describes the distribution of vibrational states for an excited ion [37]. The larger r_1 is, as compared to r_0, the more probable will be the generation of ions excited even well above the dissociation energy. Photoelectron spectroscopy allows for both the determination of adiabatic ionization energies and of Franck-Condon factors (Chap. 2.10.4).

The counterpart of the vertical ionization is a process where ionization of the neutral in its vibrational ground state would yield the radical ion also in its vibrational ground state, i.e., the $(0 \leftarrow 0)$ transition. This is termed *adiabatic ionization* and should be represented by a diagonal line in the diagram. The difference $IE_{vert} - IE_{ad}$ can lead to errors in ionization energies in the order of 0.1–0.7 eV [7].

The further fate of the ion depends on the shape of its potential energy surface. In case there is a minimum and the level of excitation is below the energy barrier for dissociation, D, the ion can exist for a very long time. Ions having an *internal energy* above the dissociation energy level will dissociate at some point leading to causing fragment ions within a mass spectrum. In some unfavorable cases, ions bear no minimum on their energy surface at all. These will suffer spontaneous dissociation and consequently, there is no chance to observe a molecular ion.

Note: To understand the situation of the molecule imagine an apple through which a bullet is being shot: the impacting bullet passes through the apple, transfers an amount of energy, tears some of the fruit out and has long left it when the perforated apple finally drops or breaks into pieces.

2.3 Ionization Efficiency and Ionization Cross Section

The ionization energy represents the absolute minimum energy required for ionization of the neutral concerned. This means in turn that in order to effect ionization, the impacting electrons need to carry at least this amount of energy. If this energy were then to be quantitatively transferred during the collision, ionization would take place. Obviously, such an event is of rather low probability and therefore, the *ionization efficiency* is close to zero with electrons carrying just the *IE* of the pertinent neutral. However, a slight increase in electron energy brings about a steady increase in ionization efficiency.

Strictly speaking, every molecular species has an ionization efficiency curve of its own depending on the *ionization cross section* of the specific molecule. In the case of methane, this issue has been studied repeatedly (Fig. 2.5) [12]. The ionization cross section describes an area through which the electron must travel in order to effectively interact with the neutral and consequently, the ionization cross section is given in units of square-meters.

Fortunately, the curves of ionization cross section vs. electron energy are all of the same type, exhibiting a maximum at electron energies around 70 eV (Fig. 2.5). This explains why EI spectra are almost always acquired at 70 eV.

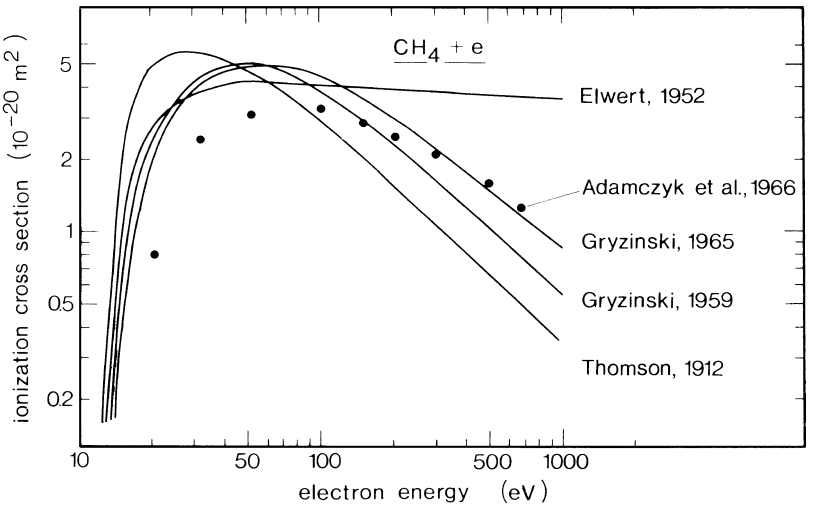

Fig. 2.5. Ionization cross sections for CH_4 upon electron ionization as obtained by several research groups. Reproduced from Ref. [12] with permission. © Elsevier Science, 1982.

Reasons for measuring EI spectra at 70 eV:

- All atoms or molecules can be ionized at 70 eV, whereas at 15 eV such gases as He, Ne, Ar, H_2, and N_2 are not.
- The plateau of the ionization efficiency curve at ~70 eV implies small that variations in electron energy are negligible; actually EI at 60–80 eV work just as well.
- Therefore: better reproducibility of spectra, allowing comparison of spectra obtained from different mass spectrometers or from mass spectral databases (Chap 5.8).

2.4 Internal Energy and the Further Fate of Ions

When an analyte is transferred into the ion source by means of any kind of sample introduction system it is in thermal equilibrium with this inlet device. As a result, the energy of the incoming molecules is represented by their thermal energy. This is the last opportunity to control the temperature, being a macroscopic property. After that, gas phase dilution would preclude any further collisions from taking place, and accordingly, any intermolecular energy transfer that would provide the basis for reaching thermal equilibrium and the validity of the *Boltzmann distribution* governing condensed phases and normal pressure gas phases. Thus, ionization changes the situation dramatically, as comparatively large amounts of energy need to be "handled" internally by the freshly formed ion. Even though part of this energy will contribute to translational or rotational energy of the molecule as a whole, the major fraction has to be stored in internal modes. Among the internal

modes rotational excitation cannot store significant amounts of energy, whereas vibration and especially electronic excitation are capable of an uptake of several electronvolts each [38,39].

2.4.1 Degrees of Freedom

Any atom or molecule in the gas phase has *external degrees of freedom*, because atoms and molecules as a whole can move along all three dimensions in space (along x, y, and z directions). This yields three *translational degrees of freedom*. From the kinetic gas theory the average translational energy can easily be estimated as $^3/_2kT$ delivering 0.04 eV at 300 K and 0.13 eV at 1000 K.

In case of diatomic and other linear molecules there are two rotations (around the x and y axes) and for all other molecules three rotations (around the x, y, and z axes). Thus, we have two or three more degrees of freedom contributing another kT or $^3/_2kT$ of energy, respectively, for the latter summing up to 0.08 eV at room temperature and 0.26 eV at 1000 K. This does not change independently of the number of atoms of the molecule or of their atomic masses.

In contrast to the external degrees of freedom, the number of *internal degrees of freedom*, notably *vibrational degrees of freedom*, s, increases with the number of atoms within the molecule, N. These internal degrees of freedom represent the number of vibrational modes a molecule can access. In other words, each of N atoms can move along three coordinates in space yielding $3N$ degrees of freedom in total, but as explained in the preceding paragraph, three of them have to be subtracted for the motion of the molecule as a whole and an additional two (linear) or three (nonlinear) have to be subtracted for rotational motion as a whole. Thus, we obtain for the number of vibrational modes

$$s = 3N - 5 \quad \text{in case of diatomic or linear molecules} \tag{2.8}$$

$$s = 3N - 6 \quad \text{in case of nonlinear molecules.} \tag{2.9}$$

It is obvious that even relatively small molecules possess a considerable number of vibrational modes.

Example: The thermal energy distribution curves for 1,2-diphenylethane, $C_{14}H_{14}$, $s = 3 \times 28 - 6 = 78$, have been calculated at 75 and 200 °C [40]. Their maxima were obtained at ~0.3 and ~0.6 eV, respectively, with almost no molecules exceeding twice that energy of maximum probability. At 200 °C, the most probable energy roughly corresponds to 0.008 eV per vibrational degree of freedom, which is a very small as compared to binding energies.

This indicates that excited vibrational states are almost fully unoccupied at room temperature and only the energetically much lower-lying internal rotations are effective under these conditions. Upon electron ionization, the situation changes quite dramatically as can be concluded from the Franck-Condon principle and therefore, energy storage in highly excited vibrational modes becomes of key importance for the further fate of ions in a mass spectrometer. In case of an indene

molecule having 45 vibrational modes, the storage of 10 eV would mean roughly 0.2 eV per vibration, i.e., roughly a 20-fold value of thermal energy, provided the energy is perfectly randomized among the bonds.

2.4.2 Appearance Energy

As explained by the Franck-Condon diagram, hardly any molecular ions will be generated in their vibrational ground state. Instead, the majority of the ions created by EI is vibrationally excited and many of them are well above the dissociation energy level, the source of this energy being the 70 eV electrons. Dissociation of $M^{+\bullet}$, or fragmentation as it is usually referred to in mass spectrometry, leads to the formation of a fragment ion, m_1^+, and a neutral, generally referred to as

$$M^{+\bullet} \rightarrow m_1^+ + n^\bullet \tag{2.10}$$

$$M^{+\bullet} \rightarrow m_1^{+\bullet} + n \tag{2.11}$$

Reaction 2.10 describes the loss of a radical, whereas reaction 2.11 corresponds to the loss of a molecule, thereby conserving the radical cation property of the molecular ion in the fragment ion. Bond breaking is a endothermal process and thus the potential energy of the fragment ion is usually located at a higher energy level (Fig. 2.6).

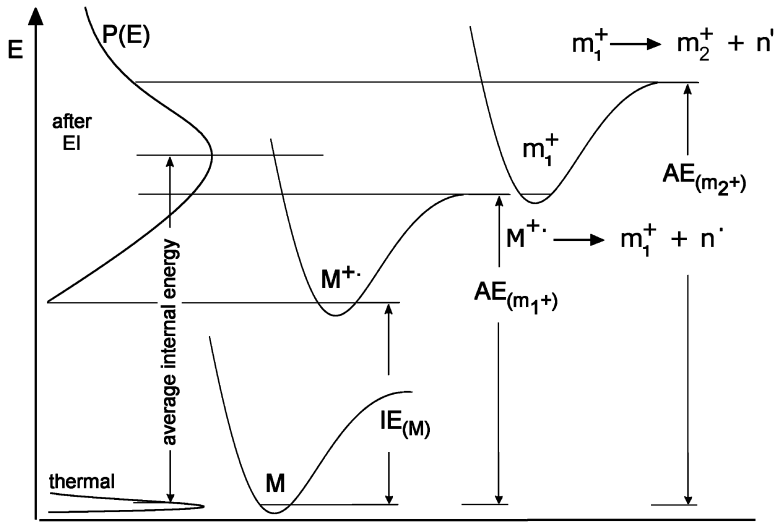

Fig. 2.6. Definition of the appearance energy and visualization of changes in internal energy distributions, $P_{(E)}$, of relevant species upon electron ionization and subsequent fragmentation (energy scale compressed for the ions).

Definition: The amount of energy needed to be transferred to the neutral M to allow for the detection of the fragment ion m_1^+ is called the *appearance energy* (*AE*) of that fragment ion. The old, and also incorrect, term *appearance potential* (*AP*) is still found in the literature.

In fact, the ions are not generated by one specific internal energy applying for all ions, but via a broad energy distribution $P_{(E)}$. One should keep in mind, however, that such a distribution is only valid for a large set of ions as each individual one bears a defined internal energy, ranging from just above *IE* to well beyond 10 eV for certain ones. Fragmentation of those highly excited ions from the tail of the $P_{(E)}$ curve yields fragment ions having still enough energy for a second dissociation step, $m_1^+ \rightarrow m_2^+ + n'$ or even a third one. Each of the subsequent steps can in principle also be characterized by an appearance energy value.

2.4.3 Bond Dissociation Energies and Heats of Formation

Great efforts have been made to generate accurate and reliable ion thermochemistry data. Once such data is available, it can be employed to elucidate fragmentation mechanisms and in addition, it is useful for obtaining some background on the energetic dimensions in mass spectrometry.

Heats of formation of neutral molecules, $\Delta H_{f(RH)}$, can be obtained from combustion data with high accuracy. Bond dissociation energies can either be derived for *homolytic bond dissociation*

$$R\text{–}H \rightarrow R^{\bullet} + H^{\bullet}, \ \Delta H_{Dhom} \tag{2.12}$$

or *heterolytic bond dissociation*

$$R\text{–}H \rightarrow R^{+} + H^{-}, \ \Delta H_{Dhet} \tag{2.13}$$

The homolytic bond dissociation enthalpies give the energy needed to cleave a bond of the neutral molecule which, in the gas phase is in its vibrational and electronic ground states, to obtain a pair of radicals which also are not in excited modes. Homolytic bond dissociation enthalpies are in the range of 3–5 eV (Table 2.2). The heterolytic bond dissociation energies apply for the case of creating a cation and an anion in their ground states from the neutral precursor which means that these values include the amount of energy needed for charge separation; they are in the order of 10–13 eV (Table 2.3). Due to the significantly altered bonding situation, breaking of a bond is clearly less demanding in molecular ions than in neutral molecules.

Example: The minimum energy needed to form a CH_3^+ ion and a hydrogen radical from the methane molecular ion can be estimated from the heat of reaction, ΔH_r, of this process. According to Fig. 2.6, $\Delta H_r = AE_{(CH3+)} - IE_{(CH4)}$. In order to calculate the missing $AE_{(CH3+)}$ we use the tabulated values of $\Delta H_{f(H^{\bullet})} = 218.0$ kJ mol^{-1}, $\Delta H_{f(CH3+)} = 1093$ kJ mol^{-1}, $\Delta H_{f(CH4)} = -74.9$ kJ mol^{-1}, and $IE_{(CH4)} = 12.6$ eV

= 1216 kJ mol^{-1}. First, the heat of formation of the methane molecular ion is determined:

$$\Delta H_{f(CH4+\bullet)} = \Delta H_{f(CH4)} + IE_{(CH4)} \tag{2.14}$$

$$\Delta H_{f(CH4+\bullet)} = -74.9 \text{ kJ mol}^{-1} + 1216 \text{ kJ mol}^{-1} = 1141.1 \text{ kJ mol}^{-1}$$

Then, the heat of formation of the products is calculated from

$$\Delta H_{f(prod)} = \Delta H_{f(CH3+)} + \Delta H_{f(H\bullet)} \tag{2.15}$$

$$\Delta H_{f(prod)} = 1093 \text{ kJ mol}^{-1} + 218 \text{ kJ mol}^{-1} = 1311 \text{ kJ mol}^{-1}$$

Now, the heat of reaction is obtained from the difference

$$\Delta H_r = \Delta H_{f(prod)} - \Delta H_{f(CH4+\bullet)} \tag{2.16}$$

$$\Delta H_r = 1311 \text{ kJ mol}^{-1} - 1141.1 \text{ kJ mol}^{-1} = 169.9 \text{ kJ mol}^{-1}$$

The value of 169.9 kJ mol^{-1} (1.75 eV) corresponds to $AE_{(CH3+)} = 14.35$ eV which is in good agreement with published values of about 14.3 eV [23,45]. In addition, this is only 40% of the homolytic C–H bond dissociation enthalpy of the methane molecule, thereby indicating the weaker bonding in the molecular ion.

Table 2.2. Homolytic bond dissociation enthalpies, ΔH_{Dhom}, and heats of formation, $\Delta H_{f(X\bullet)}$, of some selected bonds and radicals [kJ mol^{-1}] [a]

	X$^\bullet$	H$^\bullet$	$CH_3^\bullet$	Cl$^\bullet$	OH$^\bullet$	$NH_2^\bullet$
	$\Delta H_{f(X\bullet)}$	218.0	143.9	121.3	37.7	197.5
R$^\bullet$	$\Delta H_{f(R\bullet)}$					
H$^\bullet$	218.0	436.0	435.1	431.4	497.9	460.2
$CH_3^\bullet$	143.9	435.1	373.2	349.8	381.2	362.8
$C_2H_5^\bullet$	107.5	410.0	354.8	338.1	380.3	352.7
i-$C_3H_7^\bullet$	74.5	397.5	352.3	336.4	384.5	355.6
t-$C_4H_9^\bullet$	31.4	384.9	342.3	335.6	381.6	349.8
$C_6H_5^\bullet$	325.1	460.1	417.1	395.4	459.0	435.6
$C_6H_5CH_2^\bullet$	187.9	355.6	300.4	290.4	325.9	300.8
$C_6H_5CO^\bullet$	109.2	363.5	338.1	336.8	440.2	396.6

[a] Values from Ref. [41]

The heat of formation of organic radicals and positive ions decreases with their size and even more importantly with their degree of branching at the radical or ionic site. A lower heat of formation is equivalent to a higher thermodynamic stability of the respective ion or radical. The corresponding trends are clearly expressed by the values given in Tables 2.2 and 2.3. This causes the fragmentation pathways of molecular ions proceeding by formation of secondary or tertiary radi-

cals and/or ions to become dominant over those leading to smaller and/or primary radical and ionic fragments, respectively (Chap. 6.2.2).

Example: An impressive case showing the effects of isomerization upon thermal stability is that of butyl ions, $C_4H_9^+$. This carbenium ion can exist in four isomeric states with heats of formation that range from 837 kJ mol^{-1} in the case of *n*-butyl over 828 kJ mol^{-1} for *iso*-butyl (also primary) to 766 kJ mol^{-1} for *sec*-butyl to 699 kJ mol^{-1} in the case of *t*-butyl, meaning an overall increase in thermodynamic stability by 138 kJ mol^{-1} (Chap. 6.6.2) [42].

Table 2.3. Heterolytic bond dissociation enthalpies, ΔH_{Dhet}, and heats of formation of some molecules and ions [kJ mol^{-1}] [a]

Ion	ΔH_{Dhet}	$\Delta H_{f(R+)}$	$\Delta H_{f(RH)}$
Proton, H^+	1674	1528	0.0
Methyl, CH_3^+	1309	1093	–74.9
Ethyl, $C_2H_5^+$	1129	903	–84.5
n-Propyl, $CH_3CH_2CH_2^+$	1117	866	–103.8
i-Propyl, $CH_3CH^+CH_3$	1050	802	–103.8
n-Butyl, $CH_3CH_2CH_2CH_2^+$	1109	837	–127.2
sec-Butyl, $CH_3CH_2CH^+CH_3$	1038	766	–127.2
i-Butyl, $(CH_3)_2CHCH_2^+$	1109	828	–135.6
t-Butyl, $(CH_3)_3C^+$	975	699	–135.6
Phenyl, $C_6H_5^+$	1201	1138	82.8

[a] Values from Refs. [8,42-44]

2.4.4 Randomization of Energy

The best evidence for randomization of internal energy over all vibrational modes of a molecular ion prior to any fragmentation is delivered by EI mass spectra themselves. If there was no randomization, fragmentation would occur directly at any bond that immediately suffers from the withdrawal of an electron. As a result, mass spectra would show an almost statistical bond breaking throughout the molecular ion. Instead, mass spectra reveal a great deal of selectivity of the molecular ion when choosing fragmentation pathways. This means the molecular ion explores many pathways up to its respective transition states and prefers the thermodynamically (and as we will see, also kinetically) more favorable ones. The same is true for fragment ions.

From a purely thermodynamic point of view the situation can be elucidated by considering a hypothetical molecular ion having some internal energy and being faced to the selection of a fragmentation pathway (Fig. 2.7).

a) The molecular ion $ABC^{+\bullet}$ has an internal energy E_{inta} being slightly above the activation energy, E_{02}, required to cross the transition state TS_2 leading to the

formation of $A^{\bullet}$ and BC^{+}, but definitely more than needed to dissociate into AB^{+} and $C^{\bullet}$. The difference between the energy content E_{inta} and E_{01} is termed *excess energy*, $E_{ex} = E_{int} - E_0$, of the transition state TS_1. In this case either ionic product would be observed, but the third pathway could not be accessed.

b) The molecular ion $ABC^{+\bullet}$ has an internal energy E_{intb} being clearly higher than any of the three activation energies. Here, formation of all possible products should occur.

A simple comparison of activation energies does not allow, however, to predict the relative intensities of the ions AB^{+} and BC^{+} or of AB^{+}, BC^{+}, and A^{+}, respectively. In fact, from this model one would expect similar or even equal abundances of all accessible fragment ions. Actual mass spectra show greatly differing intensities of signals resulting from competing decomposition pathways. This reveals the oversimplification of the preceding passage.

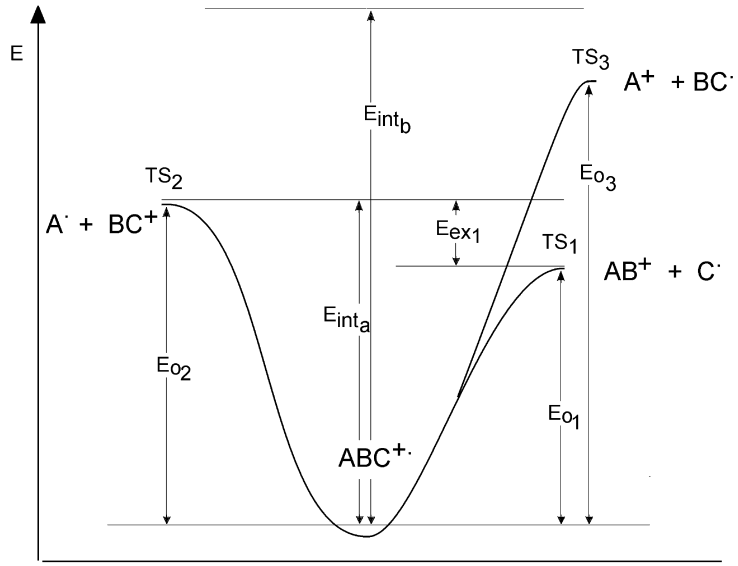

Fig. 2.7. Competition of fragmentation pathways strongly depends on the internal energy of the fragmenting ion and on the activation energies, E_0, of the transition states, i.e., the "energy barriers" of the respective reactions.

Note: Thermodynamic data such as heats of formation and activation energies alone are not sufficient to adequately describe the unimolecular fragmentations of excited ions.

2.5 Quasi-Equilibrium Theory

The *quasi-equilibrium theory* (QET) of mass spectra is a theoretical approach for describing the unimolecular decompositions of ions and hence their mass spectra [46-48]. QET is an extention of the Rice-Ramsperger-Marcus-Kassel (RRKM) theory with the aim of accommodating the conditions of mass spectrometry and marks a landmark in the theory of mass spectra [11]. Within the mass spectrometer almost all processes occur under high vacuum, i.e., in the highly diluted gas phase – one needs to be aware of how this contrasts to chemical reactions in the condensed phase as usually carried out in the laboratory [49,50]. In essence, bimolecular reactions rarely occur in a mass spectrometer and we are rather dealing with the chemistry of *isolated ions in the gas phase*. Isolated ions are not in thermal equilibrium with their surrounds as assumed by the RRKM theory. Instead, to be isolated in the gas phase means for an ion that it may only internally redistribute energy and that it may only undergo unimolecular reactions such as isomerization or dissociation. This is why the theory of unimolecular reactions is of paramount importance in mass spectrometry.

QET is not the sole theory in the field; indeed, there are several apparently competitive statistical theories for describing rate constants of unimolecular reactions [10,48]. However, none of these theories has been able to quantitatively describe all reactions of a given ion. QET, however, is well established and even in its simplified form allows sufficient insight into the behavior of isolated ions. Thus, we start out the chapter from the basic assumptions of QET. Along this scheme we will be led from the neutral molecule to ions, and from transition states and reaction rates to fragmentation products and thus, through the basic concepts and definitions of gas phase ion chemistry.

2.5.1 QET's Basic Premises

According to QET the rate constant, k, of a unimolecular reaction is basically a function of excess energy, E_{ex}, of the reactants in the transition state and thus $k_{(E)}$ strongly depends on the internal energy distribution of any particular ion. QET is thus based on the following essential premises [46,51]:

1. The initial ionization is "vertical", i.e., there is no change of position or kinetic energy of the nuclei while it is taking place. With the usual electron energy any valence shell electron may be removed.
2. The molecular ion will be of low symmetry and have an odd electron. It will have as many low-lying excited electronic states as necessary to form essentially a continuum. Radiationless transitions then will result in transfer of electronic energy into vibrational energy at times comparable to the periods of nuclear vibrations.
3. These low-lying excited electronic states will in general not be repulsive; hence, the molecular ions will not dissociate immediately, but rather remain to-

gether for a time sufficient for the excess electronic energy to become randomly distributed as vibrational energy over the ion.
4. The rates of dissociation of the molecular ion are determined by the probabilities of the energy randomly distributed over the ion becoming concentrated in the particular fashions required to give several activated complex configurations yielding the dissociations.
5. Rearrangements of the ions can occur in a similar fashion.
6. If the initial molecular ion has sufficient energy, the fragment ion will in turn have enough energy to undergo further decomposition.

The characteristics of the ionization process as described in Chap. 2.2 justify the first assumption of QET. Further, it is obvious that electronic excitation occurs together with vibrational excitation and thus, the second assumption of QET is met.

2.5.2 Basic QET

QET focuses on the dynamic aspects of ion fragmentation. It describes the *rate constants* for the dissociation of isolated ions as a function of internal energy, E_{int}, and activation energy of the reaction, E_0. By doing so, it compensates for the shortcomings of the merely thermodynamic treatment above.

QET delivers the following expression for the unimolecular rate constant

$$k_{(E)} = \int_0^{E-E_0} \frac{1}{h} \times \frac{\rho^*_{(E_{\text{int}},E_0,E_t)}}{\rho_{(E)}} dE_t \tag{2.17}$$

In this equation, $\rho_{(E)}$ is the density of energy levels for the system with total energy E_{int}, and $\rho_{(E,E0,Et)}$ is the density of energy levels in the activated complex, i.e., transition state, with activation energy E_0 and translational energy E_t in the reaction coordinate. The reaction coordinate represents the bond which is actually being broken. The expression is slightly simplified by approximating the system by as many harmonic oscillators as there are vibrational degrees of freedom

$$k_{(E)} = \left(\frac{E_{\text{int}} - E_0}{E_{\text{int}}} \right)^{s-1} \frac{\prod_{j=1}^{s} \nu_j}{\prod_{i=1}^{s-1} \nu_i^*} \tag{2.18}$$

Then, the exponent is given by the number of degrees of freedom, s, minus 1 for the breaking bond. For a strict treatment of fragmenting ions by QET one would need to know the activation energies of all accessible reactions and the probability functions describing the density of energy levels.

In the most simplified form, the rate constant $k_{(E)}$ can be expressed as

$$k_{(E)} = \nu \times \left(\frac{E_{\text{int}} - E_0}{E_{\text{int}}} \right)^{s-1} \tag{2.19}$$

where ν is a frequency factor which is determined by the number and density of vibrational states. The frequency factor thereby replaces the complex expression of probability functions. Now, it becomes clear that a reaction rate considerably increases with growing E_{ex}.

$$k_{(E)} = \nu \times \left(\frac{E_{ex}}{E_{\text{int}}} \right)^{s-1} \tag{2.20}$$

Unfortunately, as with all oversimplified theories, there are limitations for the application of the latter equation to ions close to the dissociation threshold. In these cases, the number of degrees of freedom has to be replaced by an effective number of oscillators which is obtained by use of an arbitrary correction factor [7]. However, as long as we are dealing with ions having internal energies considerably above the dissociation threshold, i.e., where $(E - E_0)/E \approx 1$, the relationship is valid and can even be simplified to give the quasi-exponential expression

$$k_{(E)} = \nu \times e^{-(s-1)E_0/E} \tag{2.21}$$

Example: For $\nu = 10^{15}$ s^{-1}, $s = 15$, $E_{\text{int}} = 2$ eV, and $E_0 = 1.9$ eV the rate constant is calculated as 3.0×10^{-5} s^{-1}. For the same parameters but $E_{\text{int}} = 4$ eV we obtain $k = 6.3 \times 10^{10}$ s^{-1} being a 2.1×10^{15}-fold increase. This means that a reaction is extremely slow at small excess energies but becomes very fast as soon as there is some substantial excess energy available.

2.5.3 Rate Constants and Their Meaning

The rate constants of unimolecular reactions have the dimension *per second* (s^{-1}). This means the process can happen x times per second, e.g., $k = 6.3 \times 10^{10}$ s^{-1} being equivalent to 1.6×10^{-11} s *per fragmentation on the average*. Note the emphasis "on the average", because rate constants are macroscopic and statistical in nature as they get their meaning only from considering a very large number of reacting particles. A single ion will have a lifetime of 1.6×10^{-11} s *on the average* in this case; however, a specific one in consideration might also decay much sooner or later, with the actual decay occurring at the speed of vibrational motions. The dimension s^{-1} also means there is no dependence on concentration as it is the case with second- or higher order reactions. This is because the ions are isolated in the gas phase, alone for their entire lifetime, and the only chance for change is by means of unimolecular reaction.

2.5.4 $k_{(E)}$ Functions – Typical Examples

Although the general shape of any $k_{(E)}$ function resembles the ionization efficiency curve to the left of the maximum, these must not be confused. At an excess energy close to zero, the rate constant is also close to zero but it rises sharply upon slight increase of the excess energy. However, there is an upper limit for the rate of a dissociation that is defined by the vibrational frequency of the bond to be cleaved. The fragments are not able to fly apart at a higher velocity than determined by their vibrational motion (Fig. 2.8).

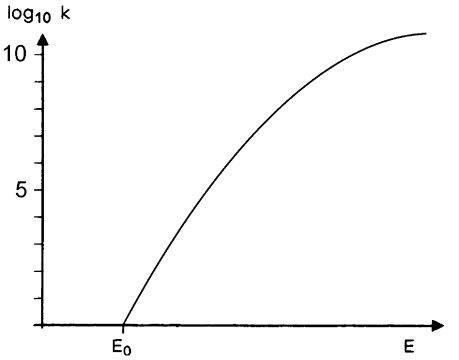

Fig. 2.8. General shape of a log k vs. E plot as determined by the simplified QET. At $E = E_0$ the reaction is extremely slow. A slight increase in energy causes k to rise sharply.

2.5.5 Reacting Ions Described by $k_{(E)}$ Functions

According to our knowledge of rate constants, Fig. 2.7 requires a different interpretation. At an internal energy E_{inta} the molecular ion $ABC^{+\bullet}$ can easily cross the transition state TS_1 to form AB^+ and $C^\bullet$. The products of the second reaction can in principle be formed, even though the excess energy at TS_2 is so small that the product ion BC^+ will almost be negligible. The third pathway is still not accessible. At an internal energy E_{intb} the excess energy is assuredly high enough to allow for any of the three pathways with realistic rates to observe the products. Nevertheless, due to the strong dependence of the rate constant on E_{ex}, the reaction over TS_3 will be by far the least important.

2.5.6 Direct Cleavages and Rearrangement Fragmentations

The reactions of excited ions are not always as straightforward as expected. Of course, the existence of multiple fragmentation pathways for an ion consisting of several tens of atoms brings about different types of reactions all of which certainly will not lead to the same $k_{(E)}$ function [52].

The $k_{(E)}$ functions of two reactions of the same type, appear to be "parallel" in comparison, starting out at different activation energies (Fig. 2.9a), whereas different types of reactions will show a crossover of their $k_{(E)}$ functions at intermediate excess energy (Fig. 2.9b).

For example, case (**a**) depicts two competing homolytic bond cleavages. Homolytic bond cleavages are simple fragmentations of molecular ions creating an even-electron ion and a radical. One cleavage might require a somewhat higher activation energy than the other ($E_{02} > E_{01}$) because of the difference between the bonds to be cleaved, but once having enough excess energy their rates will rise sharply. The more energy is pushed into the ion, the faster the bond rupture can occur. A further increase of excess energy will become ineffective onlywhen the rate approaches the upper limit as defined by the vibrational frequency of the bond to be cleaved.

Case (**b**) compares a *rearrangement fragmentation* (reaction 1) with a *homolytic bond cleavage* (reaction 2). During a rearrangement fragmentation the precursor ion expels a neutral fragment which is an intact molecule after having rearranged in an energetically favorable manner. Rearrangements begin at low excess energy, but then the rate approaches the limit relatively soon, while cleavage starts out later, then overrunning the other at higher excess energy. The differences can be explained by the different transition states of both types of reactions. The cleavage has a *loose transition state* [40], i.e., there is no need for certain parts of the molecule to assume a specific position while the cleavage proceeds. The dissociation merely requires enough energy in the respective bond so that the binding forces can be overcome. Once the bond is stretched too far, the fragments drift apart. The rearrangement demands less excess energy to proceed, because the energy for a bond rupture on one side is compensated for by the energy received

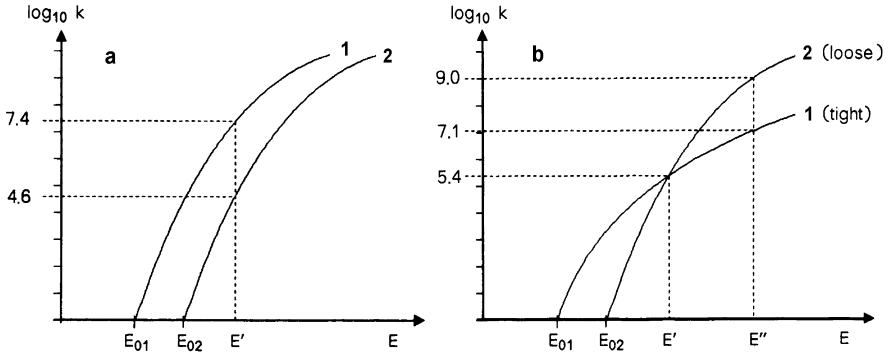

Fig. 2.9. Comparison of different types of reactions by their $k_{(E)}$ functions. (**a**) Reactions of the same type show $k_{(E)}$ functions that are "parallel", whereas (**b**) $k_{(E)}$ functions of different types tend to cross over at intermediate excess energy. In (**a**), reaction **1** would proceed $10^{2.8}$ (630) times faster at an internal energy E' than would reaction **2**. In (**b**), both reactions have the same rate constant, $k = 10^{5.4}$ s^{-1}, at an internal energy E', whereas reaction **2** becomes $10^{1.9}$ (80) times faster at E''.

when a new bond is formed by the accepting position. Compared to the simple cleavage, such a transition state is usually termed *tight transition state* (cf. Chap. 6.12.2). Then, the neutral is expelled in a second step. Such a reaction obviously depends on the suitable conformation for rearrangement at the same time when sufficient energy is put into the bond to be cleaved. Furthermore, the second step has to follow in order to yield the products. Overall, there is no use in having more than enough energy until the ion reaches the conformation needed. Thus, after considering either basic type of fragmentation, the fifth assumption of QET is justified, because there is no reason why rearrangements should not be treated by QET.

2.6 Time Scale of Events

We have just learned that ionization occurs on the low femtosecond timescale, direct bond cleavages require between some picoseconds to several tens of nanoseconds, and rearrangement fragmentations usually proceed in much less than a microsecond (Fig. 2.10). All those chemical reactions are strictly unimolecular, because the reacting ions are created in the highly diluted gas phase – circumstances that prevent bimolecular reactions of the ions during their residence time within the ion source. This dwell time is determined by the extraction voltages applied to accelerate and focus ions to form a beam and by the dimensions of that ion source. In standard EI sources the ions spend about 1 µs before they are ejected by action of the accelerating potential [53].

Therefore, a reaction needs to proceed within that certain period of time to make the products detectable in the mass spectrum, and for this purpose there is a need for some excess energy in the transition state.

Finally, some fragment ions may even be formed after the excited species has left the ion source, so to speak in the "afterglow", giving rise to metastable ion dissociation. As the ions then travel at speeds of some 10^4 m s^{-1} they pass the mass analyzer in the order of 10–50 µs (Fig. 2.11) [9]. Even though this particular case has been adapted for a double-focusing magnetic sector mass spectrometer, an ion of *m/z* 100, and an acceleration voltage of 8 kV, the effective time scales for other types of beam instruments (quadrupole, time-of-flight) are very similar under their typical conditions of operation (Table 2.4).

Table 2.4. Typical ion flight times in different types of mass spectrometers

Mass analyzer	Flight path [m]	Acceleration voltage [V]	Typical *m/z*	Flight time [µs]
Quadrupole	0.2	10	500	57
Magnetic sector	2.0	5000	500	45
Time-of-flight	2.0	20,000	2000	45

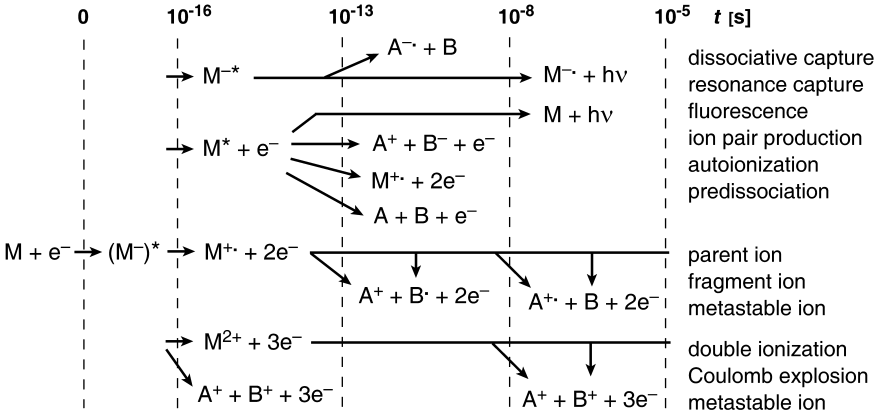

Fig. 2.10. Schematic time chart of possible electron ionization processes. Adapted from Ref. [39] with permission. © Wiley & Sons, 1986.

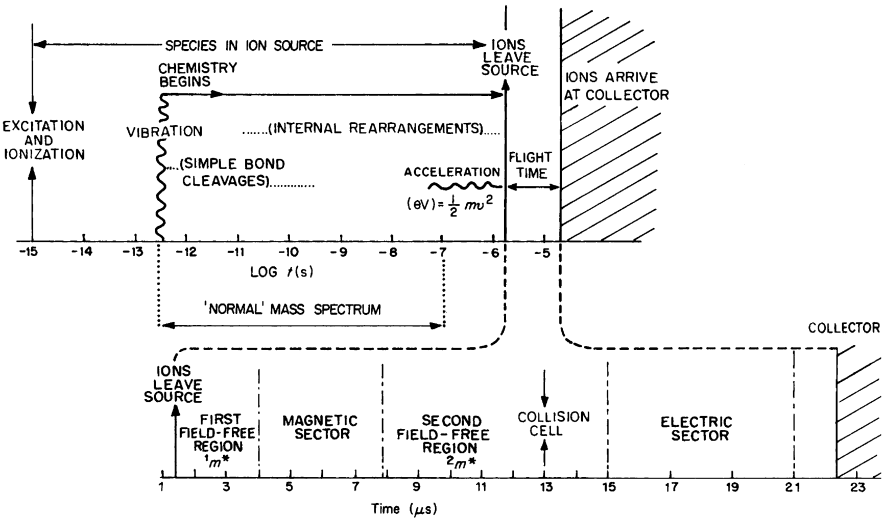

Fig. 2.11. The mass spectrometric time scale and its correlation to the classical instrumental framework. Note the logarithmic time scale for the ion source that spans nine orders of magnitude. Reproduced from Ref. [9] with permission. © John Wiley & Sons, Ltd., 1985.

2.6.1 Stable, Metastable, and Unstable Ions

The terminology for ions has been coined as a direct consequence of the classical mass spectrometric time scale. Nondecomposing molecular ions and molecular ions decomposing at rates below about $10^5\ s^{-1}$ will reach the detector without fragmentation and are therefore termed *stable ions*. Consequently, ions dissociat-

ing at rates above 10^6 s^{-1} cannot reach the detector. Instead, their fragments will be detected and thus they are called *unstable ions*. A small percentage, however, decomposing at rates of 10^5–10^6 s^{-1} will just fragment on transit through the mass analyzer – those are termed *metastable ions* (Figs. 2.10–2.12) [4,5,9].

Definition:	*stable ions*, $k < 10^5$ s^{-1} *metastable ions*, 10^5 $s^{-1} < k < 10^6$ s^{-1} *unstable ions*, $k > 10^6$ s^{-1}

There is no justification for such a classification of ion stabilities outside the mass spectrometer because almost all ions created under the conditions inside a mass spectrometer would spontaneously react in the atmosphere or in solvents. Nevertheless, this classification is useful as far as ions isolated in the gas phase are concerned and is valid independently of the type of mass analyzer or ionization method employed.

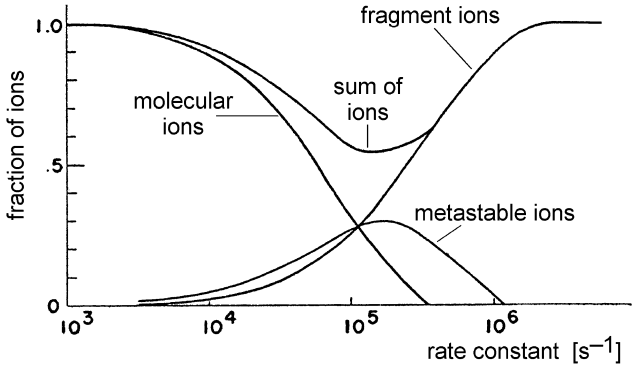

Fig. 2.12. Correlation between rate constants of ion dissociations and terminology referring to ion stability as employed in mass spectrometry. Adapted from Ref. [54] with permission. © The American Institute of Physics, 1959.

2.6.2 Time Scale of Ion Storage Devices

Many modern instruments make use of ion storage in some way. Linear radiofrequency multipoles can be axially segmented or equipped with trapping plates to their ends to raise switchable potential walls that allow to accumulate, store and eject ion packages as required. The most prominent of those devices is the *linear (quadrupole) ion trap* (LIT). The other type, the so-called *three-dimensional quadrupole ion trap* (QIT) stores ion clouds to have them ready for mass analysis by bringing them successively from stable to unstable ion trajectories that end up with ejection from the trap onto a detector. *Fourier transform ion cyclotron resonance* (FT-ICR) relies on storage of ions on circular paths to detect the angular frequencies of coherent ion packages as they repeatedly pass a pair of detection plates. The recent *orbitrap* mass analyzer employs a different operational concept

but shares the time frame with FT-ICR. Even during their transport from the ion source to the mass analyzer of the above instruments, ions are often repeatedly being accumulated, stored and passed to another section of the instrument before they finally enter the compartment for *m/z* analysis. (For details of mass analyzers refer to Chap. 4.)

The time span of ion accumulation can easily extend from milliseconds to seconds, the passage between functional units of the instrument may take tens of microseconds to milliseconds, and the *m/z* analysis requires storage times from milliseconds (QIT, LIT) to seconds (FT-ICR, orbitrap).

This way, modern mass spectrometry instrumentation has gone beyond the classical mass spectrometric time scale. Especially the time frame after leaving the ion source has drastically been extended. It is still important, however, to understand the considerations of the classical mass spectrometric time scale as it governs the processes in many types of ion sources (electron ionization, chemical ionization, field ionization and field desorption, laser desorption) and as it is still basically valid for a wide range of mass analyzers. One should be aware though of the 10^3–10^6-fold expansion of the time scale for cases where ion storage is involved. Furthermore, the handling of ions on the extended time scale is only possible if they are stable, i.e., nondecomposing, and this is in accordance with our previous definition of ion stability in terms of being just below threshold for dissociation during their dwell time in the instrument. Without the use of extremely soft ionization techniques (such as electrospray ionization), those ion-storing instruments would not have any ions to store nor to be analyzed.

2.7 Internal Energy – Practical Implications

Even comparatively small molecular ions can exhibit a substantial array of first-, second-, and higher-generation fragmentation pathways due their internal energy in the order of several electronvolts [52]. Typically, ion dissociations are endothermic, and thus each fragmentation step consumes some of the ions' internal energy. Highly excited ions may carry enough internal energy to allow for several consecutive cleavages, whereas others may just undergo one or even none (Chap. 2.4.2). The latter reach the detector as still intact molecular ions. The fragmentation pathways of the same generation compete with each other, their products being potential precursors for the next generation of fragmentation processes.

Example: Imagine the hypothetical molecular ion $ABYZ^{+\bullet}$ undergoing three competing first-generation fragmentations, two of them rearrangements, one a homolytic bond cleavage (Fig. 2.13). Next, three first-generation fragment ions have several choices each, and thus the second-generation fragment ions $Y^{+\bullet}$ and YZ^+ are both formed on two different pathways. The formation of the same higher-generation fragment ion on two or more different pathways is a widespread phenomenon. A closer look reveals that $Y^{+\bullet}$ and Y^+ are different although having identical empirical formulas, because one of them is an odd-electron and the other

an even-electron species. Nevertheless, they would both contribute to one common peak at the same nominal *m/z* in a mass spectrum of ABYZ (Chap. 3.1.4).

In an EI mass spectrum of ABYZ, all ionic species would be detected which are formed as a result of numerous competing and consecutive reactions, but there is no simple rule which of them should give rise to intensive peaks and which of them would be hardly noticed.

Obviously, the first-generation fragment ions should be more closely related to the initial structure of ABYZ than those of the second or even third generation. Fortunately, such higher generation (and therefore low-mass) fragment ions can also reveal relevant information on the constitution of the analyte. In particular, they yield reliable information on the presence of functional groups (Chap. 6).

Fragmentation trees similar to that shown here can be constructed from any EI mass spectrum, providing ten thousands of examples for the sixth assumption of QET, that fragment ions may again be subject to dissociation, provided their internal energy suffices.

Note: The assumptions of QET have turned into basic statements governing the behavior of isolated ions in the gas phase and thus, in mass spectrometry in general.

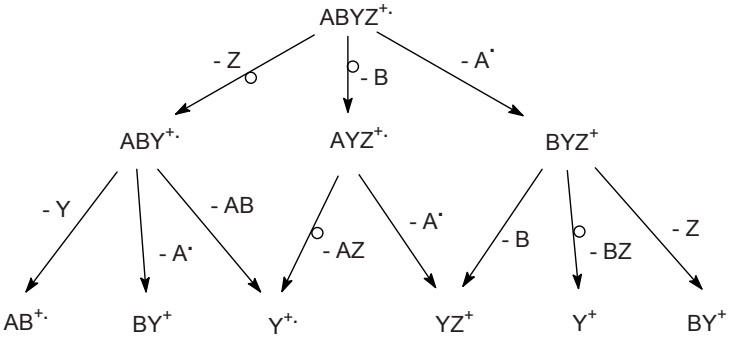

Fig. 2.13. Possible fragmentation pathways for hypothetical molecular ions $ABYZ^{+\bullet}$ having internal energies typical for EI.

2.8 Reverse Reactions and Kinetic Energy Release

2.8.1 Activation Energy of the Reverse Reaction

By merely considering thermodynamic and kinetic models we may be able to understand how ions are formed and what parameters are effective to determine their further fate in the mass spectrometer. However, the potential energy surfaces considered in this context only reached up to the transition state (Fig. 2.6). Without explicitly mentioning it, we assumed the curves to stay on the same energetic level between transition state and the products of ion dissociation, i.e., the sum of heats

of formation of the products would be equal to the energy of the transition state. This assumption is almost correct for homolytic bond cleavages in molecular ions because the recombination of an ion with a radical proceeds with almost negligible activation energy [4,5]. In other words, the *activation energy of the reverse reaction*, E_{0r} (or often simply called *reverse activation energy*) is then close to zero. This explains why the result of our simple estimation of the activation energy for hydrogen radical loss from the molecular ion of methane could be realistic (Chap. 2.4.3).

In case of rearrangement fragmentations the situation is quite different, because one of the products is an intact neutral molecule of comparatively high thermodynamic stability, i.e., having negative or at least low values of ΔH_f (Table 2.5). Once the transition state is crossed, the reaction proceeds by formation of products energetically much lower than the transition state. In case of the reverse reaction, this would require some or even substantial activation energy transfer to the fragments to allow their recombination, and thus $E_{0r} > 0$ (Fig. 2.14).

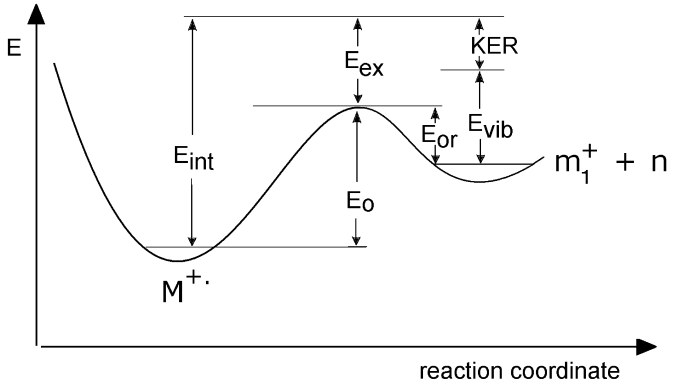

Fig. 2.14. Definition of E_{0r} and origin of KER. The excess energy of the decomposing ion in the transition state relative to the sum of the heats of formation of the ionic and neutral product is partitioned into vibrational excitation of the products plus KER.

Table 2.5. Gas phase heats of formation, ΔH_f, of some frequently eliminated molecules[a]

Molecule	ΔH_f [kJ mol^{-1}][b]	Molecule	ΔH_f [kJ mol^{-1}][b]
CO_2	–393.5	H_2CO	–115.9
HF	–272.5	HCl	–92.3
H_2O	–241.8	NH_3	–45.9
CH_3OH	–201.1	C_2H_4	52.5
CO	–110.5	HCN	135.1

[a] *IE* data extracted from Ref. [23] with permission. © NIST 2002.
[b] All values have been rounded to one digit.

2.8.2 Kinetic Energy Release

The total excess energy, E_{extot}, of the precursor ion relative to the heats of formation of the products in their ground state, comprises the excess energy in the transition state, E_{ex}, plus the activation energy of the reverse reaction, E_{0r}:

$$E_{extot} = E_{ex} + E_{0r} \tag{2.22}$$

Although most ion fragmentations are endothermic, there is still a significant amount of energy to be redistributed among the reaction products. Much of E_{extot} is redistributed as vibrational energy, E_{vib}, among the internal modes, thereby supplying the energy for consecutive fragmentation of the fragment ion. Nonetheless, some of the energy is converted into translational motion of the fragments relative to their center of gravity. This portion of E_{extot} is released in the direction of the bond that is being cleaved, in other words, into separation from each other. This is termed *kinetic energy release*, KER (Fig. 2.14) [4,5,9,55,56].

The larger the sum of $E_{ex} + E_{0r}$ the larger is the expected KER. Large reverse activation energy, especially when combined with repulsive electronic states in the transition state, will cause significant KER that has been observed up to 1.64 eV [57-60]. Significant KER also has been measured in the rare case of exothermic fragmentations [61]. On the other hand, homolytic cleavages and ion–neutral complex-mediated reactions tend to proceed with very small KER in the range of 1–50 meV (Fig. 2.15).

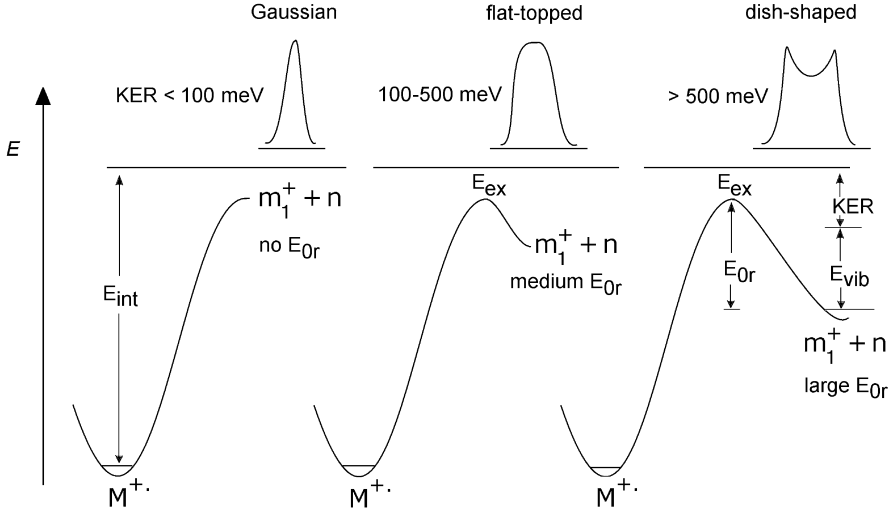

Fig. 2.15. Influence of the reverse activation energy on KER and thus, on peak shapes in metastable ion decompositions (suitable experimental setup being a prerequisite). *From left*: no or small reverse barrier causes Gaussian peak shape, whereas medium E_{0r} yields flat-topped peaks and large E_{0r} causes dish-shaped peaks.

Note: The importance of KER measurements results from the fact that the potential energy surface between transition state and products of a reaction can be reconstructed [55]. Thus, KER and *AE* data are complementary in determining the energy of the transition state.

2.8.3 Energy Partitioning

The observed KER consists of two components, one from E_{ex} and one from E_{0r}. This splitting becomes obvious from the fact that even if there is no E_{0r}, a small KER is always observed, thus demonstrating partitioning of E_{ex} between E_{vib} and E_{trans*} (KER):

$$E_{ex} = E_{vib} + E_{trans*} \tag{2.23}$$

Diatomic molecular ion dissociations represent the only case with clear energy partitioning, as all excess energy of the decomposition has to be converted to translational energy of the products ($E_{ex} = E_{trans*}$). For polyatomic ions the partitioning of excess energy can be described by a simple empirical relationship between E_{ex} and the number of degrees of freedom, s [6,62]:

$$E_{trans*} = \frac{E_{ex}}{\alpha \times s} \tag{2.24}$$

with the empirical correction factor $\alpha = 0.44$ [62]. According to Eq. 2.24 the ratio E_{trans*}/E_{ex} decreases as the size of the fragmenting ion increases. This influence has been termed *degrees of freedom effect* (DOF) [63-65].

Consequently, E_{trans*} becomes rather small for substantial values of s, e.g., 0.3 eV/(0.44 × 30) = 0.023 eV. Therefore, any observed KER in excess of E_{trans*} must originate from E_{0r} being the only alternative source [61]. The analogous partitioning of E_{0r} is described by:

$$E_{trans} = \beta E_{or} \tag{2.25}$$

with $\beta = 0.2$–0.4 and $^1/_3$ being a good approximation in many cases.

Note: In practice, most of the observed KERs (except at < 50 meV), can be attributed to E_{trans} from E_{0r} [61], and as a rule of thumb, $E_{trans} \approx 0.33\ E_{or}$

2.9 Isotope Effects

Most elements are composed of more than one naturally occurring *isotope*, i.e., having nuclei of the same *atomic number* but different *mass numbers* due to different numbers of neutrons [66]. The mass number of an isotope is given as a superscript preceding the element symbol, e.g., ^{1}H and ^{2}H (D) or ^{12}C and ^{13}C

(Chap. 3). Obviously, mass spectrometry is ideally suited for distinguishing between isotopic species, and isotopic labeling is used for mechanistic as well as analytical applications (Chap. 3.2.9). However, isotopic substitution not only affects ionic mass, but rather "isotopic substitution can have several simultaneous effects, and this complication sometimes produces results which are at first sight curious" [67].

Any effect exerted by the introduction of isotopes are termed *isotope effects*. Isotope effects can be *intermolecular*, e.g., upon $D^{\bullet}$ loss from $CD_4^{+\bullet}$ vs. $H^{\bullet}$ loss from $CH_4^{+\bullet}$, or *intramolecular*, e.g., upon $H^{\bullet}$ loss versus $D^{\bullet}$ loss from $CH_2D_2^{+\bullet}$.

2.9.1 Primary Kinetic Isotope Effects

Kinetic isotope effects represent one particular type of isotope effect. They are best rationalized when considering the potential energy diagram of both $H^{\bullet}$ and $D^{\bullet}$ loss from equivalent positions in the same isotopically labeled (e.g., deuterated) molecular ion (Fig. 2.16) [4,5,68]. The diagram is essentially symmetric, with the only differences arising from the zero-point energy (ZPE) terms. Since $H^{\bullet}$ and $D^{\bullet}$ are being lost from the same molecular ion, the single ZPE to start from is defined by this species. The transition states leading up to $H^{\bullet}$ and $D^{\bullet}$ loss possess ZPE terms associated with all the degrees of freedom of the dissociating ion except the one involved in that particular reaction. The transition state corresponding to $H^{\bullet}$ loss must therefore have a lower ZPE because it contains a C–D bond that is not involved in the actual cleavage. This corresponds to a lower ZPE than is provided by the C–H bond-retaining transition state that leads to $D^{\bullet}$ loss. Therefore, an ion with an internal energy E_{int} has a larger excess energy E_{exH} when it is about to eliminate $H^{\bullet}$ than if it cleaved off a $D^{\bullet}$. The activation energy for $H^{\bullet}$ loss is thereby lowered making it proceed faster than $D^{\bullet}$ loss ($k_H/k_D > 1$).

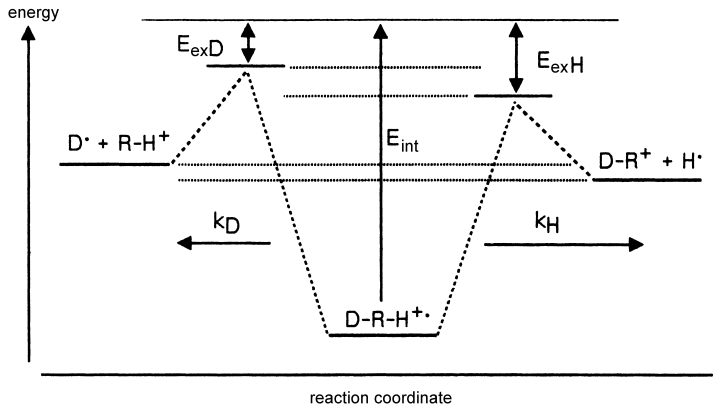

Fig. 2.16. Origin of kinetic isotope effects [4,5,68]. The change in vibrational frequencies, and thus in density of states causes somewhat higher activation energy and consequently smaller excess energy for the reaction of the deuterated bond, and thus reduces k_D.

The reason for the lower ZPE of the deuterium-retaining species is found in its lower vibrational frequencies due to the double mass of D as compared to H at almost identical binding forces. According to classical mechanics the vibrational frequency ν_D should therefore be lower by the inverse ratio of the square roots of their masses, i.e., $\nu_D / \nu_H \approx 1/1.41 \approx 0.71$ [69].

Example: Isotopic labeling does not only reveal the original position of a rearranging atom, but can also reveal the rate-determining step of multi-step reactions by its marked influence on reaction rates. Thus, the examination of H/D and $^{12}C/^{13}C$ isotope effects led to the conclusion that the McLafferty rearrangement of aliphatic ketones (Chap. 6.7) rather proceeds stepwise than concerted. [70]

Notes: *i*) The isotope effects dealt with in mass spectrometry are usually *intramolecular kinetic isotope effects*, i.e., two competing fragmentations only differing in the isotopic composition of the products exhibit different rate constants k_H and k_D [71]. *ii*) The kinetic isotope effect is called *normal* if $k_H/k_D > 1$ and *inverse* if $k_H/k_D < 1$. *iii*) Isotope effects can also be observed on KER [60,72], e.g., the KER accompanying H_2 loss from methylene immonium ion varies between 0.61 and 0.80 eV upon D labeling at various positions [60].

The term *primary kinetic isotope effect* applies if the effect is exerted on a bond where the isotope itself is involved during the reaction. It seems clear that there is no single well-defined value of the kinetic isotope effect of a reaction (Fig. 2.17) and that it strongly depends on the internal energy of the decomposing ions. In the rare case when E_{int} is just above the activation energy for $H^\bullet$ loss but still below that for $D^\bullet$ loss, the isotope effect would be infinite. As ions in a mass spectrometer usually exhibit comparatively wide distributions of E_{int}, the probability for such a case is extremely low. However, kinetic isotope effects can be large in case of decomposing metastable ions ($k_H/k_D \approx 2$–4) because these ions possess only small excess energies. Such circumstances make them sensitive to the difference between E_{exD} and E_{exH}. On the other hand, ions that decompose in the ion source usually have high internal energies, and thus smaller isotope effects are observed ($k_H/k_D \approx 1$–1.5).

While the mass of H remarkably differs from that of D (2 u/1 u = 2), the relative increase in mass is much lower for heavier elements such as carbon (13 u/12 u ≈ 1.08) [70] or nitrogen (15 u/14 u ≈ 1.07). In consequence, kinetic isotope effects of those elements are particularly small and special attention has to be devoted for their proper determination.

2.9.2 Measurement of Isotope Effects

Mass spectrometry measures the abundance of ions vs. their *m/z* ratio, and it is common practice to use the ratio $I_{mH}/I_{mD} = k_H/k_D$ as a direct measure of the isotope effect. The typical procedure for determining isotope effects from intensity ratios is to solve a set of simultaneous equations [73-76].

Example: The transfer of a D compared to the transfer of an H during propene loss from partially labeled phenylpropylethers is accompanied by an isotope effect, the approximate magnitude of which was estimated as follows [76]:

$$[1,1-D_2]: \quad \frac{[C_6H_6O]^+}{[C_6H_5OD]^+} = \frac{\alpha\, i}{1-\alpha} \tag{2.28}$$

$$[2,2,3,3,3-D_5]: \quad \frac{[C_6H_6O]^+}{[C_6H_5OD]^+} = \frac{(1-\alpha)\, i}{\alpha} \tag{2.29}$$

where α is the total fraction of H transferred from positions 2 and 3 and i is the isotope effect favoring H over D transfer. Unfortunately, the situation is more complicated if more than just one complementary pair is being studied, and an exact solution will no longer be feasible. Then, a numerical approach is required to approximate the i value [76,77].

Also, a rigorous treatment of isotope effects within the framework of QET reveals that the assumption $I_{mH}/I_{mD} = k_H/k_D$ represents a simplification [71]. It is only valid for when the studied species populate a small internal energy distribution, e.g., as metastable ions do, whereas wide internal energy distributions, e.g., those of ions fragmenting in the ion source after 70 eV electron ionization, may cause erroneous results. This is because the $k_{(E)}$ functions of isotopic reactions are not truly parallel [78], but they do fulfill this requirement over a small range of internal energies (Figs. 2.16 and 2.17)

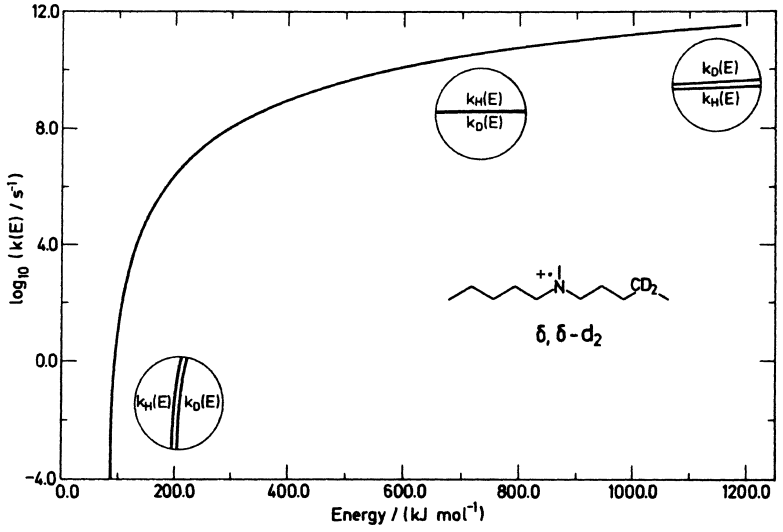

Fig. 2.17. Calculated $k_{H(E)}$ and $k_{D(E)}$ curves for the α-cleavage of deuterated amine molecular ions. The curves can be regarded as parallel over a small range of internal energies, but they are not in the strict sense. They may even cross to cause inverse isotope effects in the domain of highly excited ions. Reproduced from Ref. [78] with permission. © Wiley & Sons, 1991.

2.9.3 Secondary Kinetic Isotope Effects

Secondary kinetic isotope effects are observed if an isotopic label is located adjacent to or remote from the bond that is being broken or formed during the reaction. Again, these depend on the internal energy of the decomposing ions. Secondary kinetic isotope effects, i_{sec}, are generally much smaller than their primary analogs.

Example: The ratio $[M–CH_3]^+/[M–CD_3]^+$ from isopropylbenzene molecular ions decomposing by benzylic cleavage (Chap. 6.4) vary from 1.02 for ion source fragmentations (70 eV EI) over 1.28 for metastable ions in the 1st FFR to 1.56 in the 2nd FFR, thus clearly demonstrating the dependence of the secondary kinetic isotope effect on internal energy [79].

It is convenient to specify the value normalized *per heavier isotope present*, $i_{secnorm}$, because of the possible presence of a number of heavier isotopes, n_D [68,78]:

$$i_{sec\,norm} = \sqrt[n_D]{i_{sec}} \tag{2.30}$$

Example: Effects of a secondary kinetic isotope on the α-cleavage of tertiary amine molecular ions occurring after deuterium labeling both adjacent to and remote from the cleaved bond (Chap. 6.2.6). This reduces the fragmentation rate relative to the nonlabeled chain by factors of 1.08–1.30 per D in case of metastable ion decompositions (Fig. 2.18), but the isotope effect vanished for ion source processes [80]. The reversal of these kinetic isotope effects for short-lived ions (10^{-11}–10^{-10} s) could be demonstrated by field ionization kinetic measurements, i.e., then the deuterated species decomposed slightly faster than their nonlabeled isotopologs [68,78].

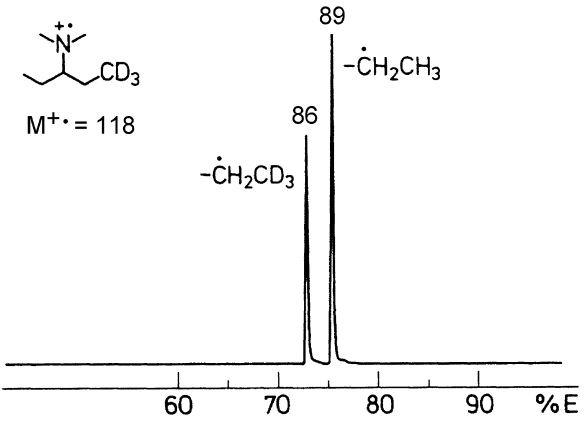

Fig. 2.18. Observation of secondary H/D isotope effects on the α-cleavage of tertiary amine molecular ions. For convenience, *m/z* labels have been added to the original energy scale of the MIKE spectrum. Adapted from Ref. [80] with permission. © American Chemical Society, 1988.

2.10 Determination of Ionization Energies

2.10.1 Conventional Determination of Ionization Energies

Ionization energies [81] can rather easily be determined – one simply needs to read out the lower limit of the electron energy at a vanishing molecular ion signal. Unfortunately, doing so yields only coarse approximations of the real ionization energy of a molecule. The accuracy of *IE* data obtained by this simple procedure will be about ± 1 eV. One of the associated problems is measuring the electron energy itself. The electrons are thermally emitted from a hot metal filament (1600–2000 °C), and therefore, their total kinetic energy is not only defined by the potential applied to accelerate them, but also by their thermal energy distribution [24]. In addition, electron ionization preferably creates vibrationally excited ions (Chap. 2.1), because ionization is a threshold process, i.e., it will take place not just when the energy needed to accomplish the process is reached, but also for all higher energies [82]. This causes a systematic error in that vertical IEs are obtained being higher than the adiabatic IEs one would like to measure. Further drawbacks are: *i*) Due to inhomogeneous electric fields within the ionization volume, the actual electron energy also depends on the location where ionization takes place. *ii*) The fact that the low electron acceleration voltages of 7–15 V have to be superimposed on the ion acceleration voltage of several kilovolts causes low precision of the voltage settings in commercial magnetic sector instruments. *iii*) There is additional thermal energy of the neutrals roughly defined by the temperature of the inlet system and the ion source.

2.10.2 Improved *IE* Accuracy from Data Post-Processing

The slightly diffuse energy of the electrons effects that the ionization efficiency curves do not approach zero in a straight line; they rather bend close to the ionization threshold and exponentially approximate zero. Even if the electron energy scale of the instrument is properly calibrated against IEs of established standards, the accuracy of the *IE* data obtained from direct readout is only ± 0.3 eV (Fig. 2.19a).

To overcome the unpredictability of the actual onset of ionization, , the *critical slope method* has been developed [24,84], among several other methods [83]. It makes use of the fact that, according to theory, realistic values of *IE* are expected at the position of the ionization efficiency curve where the slope of a semilog plot of the curve is

$$\frac{d}{dV}(\ln N_i) = \frac{n}{n+1}\,\frac{1}{kT} \tag{2.31}$$

with N_i being the total number of ions produced at an electron acceleration voltage V, and with an empirical value of $n = 2$ (Fig. 2.19b).

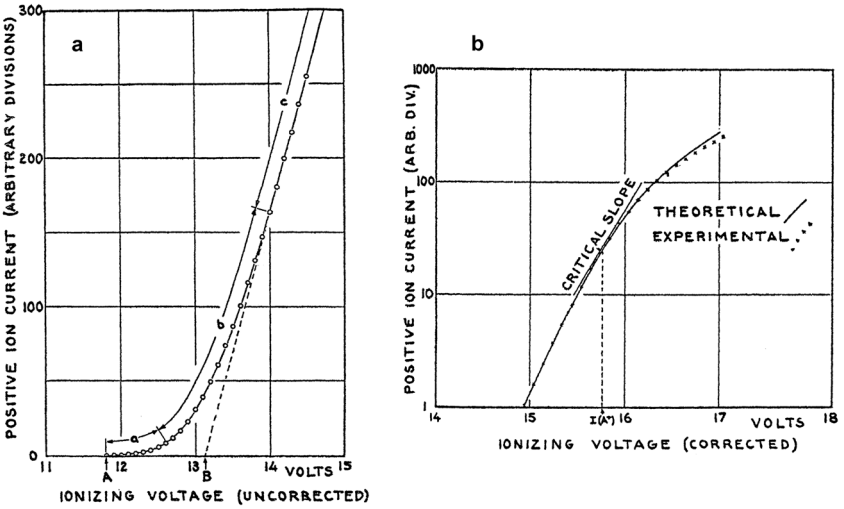

Fig. 2.19. Ionization efficiency curve of argon (**a**) plotted on a linear scale and (**b**) as semilog plot. Extrapolation of the linear portion of (**a**) gives erroneous IEs, whereas the *x*-position of the tangent of an empirical critical slope to the semilog plot yields accuracies of ± 0.05 eV. Reproduced from Ref. [24] by permission. © American Chemical Society, 1948.

2.10.3 *IE* Accuracy – Experimental Improvements

If reliable thermochemical data [23,85] is required, the above disturbing effects have to be substantially reduced. [81] One way is to use an *electron monochromator* (accuracy up to ± 0.1 eV) [86,87]. An electron monochromator is a device for selecting nearly monoenergetic electrons from an electron beam [88]. Alternatively, *photoionization* (PI) may be employed instead of EI. Photoionization yields even more accurate results (± 0.05 eV) than the electron monochromator [89]. In any case, the half width of the electron or photon energy distribution becomes small enough to detect detailed structural features of the ionization efficiency curves such as electronic transitions. Both techniques have been widely employed to obtain *IE* data (Table 1.1).

2.10.4 Photoionization Processes

The absorption of UV light by a neutral can result in electronically excited states that undergo relaxation either by emission of light or by emission of an electron. Thus, the photon in *photoionization* (PI) serves the same purpose as the energetic electron in EI.

$$M + h\nu \rightarrow M^* \rightarrow M^{+\bullet} + e^- \qquad (2.32)$$

Of course, the energy absorbed must lead into in a continuum state, i.e., at least provide the ionization energy of the neutral. Typical photon sources for PI are frequency-quadrupled Nd:Yag lasers delivering photons at 266 nm wavelength (4.6 eV) and ArF excimer lasers at 193 nm (6.3 eV). Both light sources clearly deliver photons well below the *IE* of most molecules. Fortunately, the absorption of energy has not to be a one-photon process. Instead, stepwise accumulation of energy from less energetic photons is also feasible. Thus, the normal procedure to achieve PI is *multiphoton ionization* (MUPI) [90].

The next stepping-stone to photoionization is finding the electronic levels of the neutral, because nonresonant ionization has rather low cross-sections that translate into poor ionization efficiencies along with high photon flux requirements. Resonant absorption of photons is more effective by several orders of magnitude [91]. Ideally, resonant absorption of the first photon leads to an intermediate state from where absorption of a second photon can forward the molecule into a continuum. This technique is known as 1 + 1 *resonance-enhanced multiphoton ionization* (REMPI). From a practical point of view, the second photon should be, but not necessarily has to be, of the same wavelength (Fig. 2.20) [92]. Proper selection of the laser wavelengths provides compound-selective analysis at extremely low detection limits [90,91,93,94].

Ultrashort laser pulses in the picosecond rather than the conventional nanosecond regime prevent the molecules from unwanted relaxation or fragmentation prior to molecular ion formation. The REMPI mass spectra of diphenylmercury, for example, only exhibit a molecular ion peak when sub-picosecond laser ionization is employed [95].

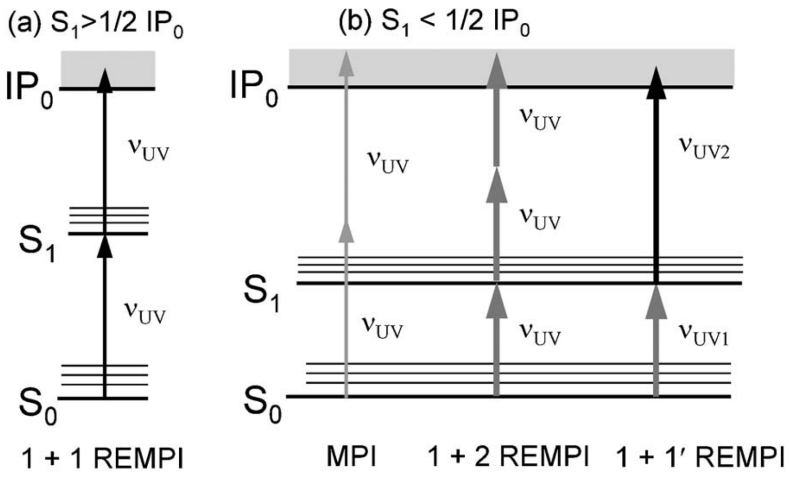

Fig. 2.20. Photoionization schemes. (**a**) Resonant 1 + 1 REMPI, (**b**) nonresonant MPI, resonant 1 + 2 REMPI, and resonant 1 + 1' REMPI with two different wavelengths. Reproduced from Ref. [92] with permission. © The Vacuum Society of Japan, 2007.

Example: The electronic and vibrational states of the oxygen molecular ion has been perfectly resolved by *photoelectron spectroscopy* (PES) (Fig. 2.21), thus allowing to directly read out the Franck-Condon factors and to identify the $(0 \leftarrow 0)$ transitions corresponding to adiabatic ionization [100].

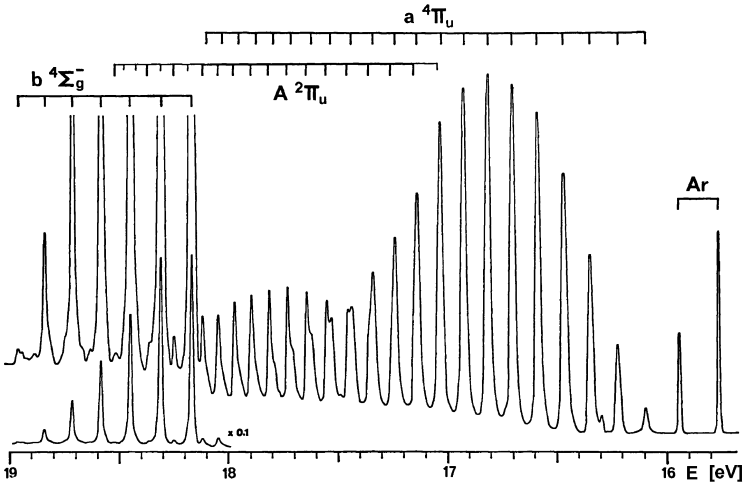

Fig. 2.21. High-resolution photoelectron spectrum of O_2, showing overlapping vibrational progressions from transitions to different electronic states of the ion (range of *IE* not shown). Reproduced from Ref. [100] with permission. © Royal Swedish Academy of Sciences, 1970.

The main disadvantage of PES and ZEKE experiments lies in the detection of electrons making the measurements sensitive to impurities, because the electrons could arise from these instead of the intended sample. This can be avoided by detecting the produced ions instead – the corresponding technique is known as *mass-analyzed threshold ionization* (MATI) [101]. In MATI experiments, the neutrals are excited in a field-free environment by means of a tunable light source (usually a multi-photon laser process) very close to the ionization threshold. Possible prompt ions are removed after about 0.1 μs by a weak positive electric field. Then, the near-threshold Rydberg species are ionized by applying a negative electric field pulse also effecting acceleration of those ions towards a time-of-flight mass analyzer [101-103]. Thus, we are finally back to a real mass spectral technique. In contrast to ZEKE, the mass selectivity of MATI allows not only for the study of molecules [101,103], but also consideration of dissociating complexes and clusters [82,104,105].

Example: The ionization spectra at the first ionization threshold of pyrazine as obtained by PI, MATI, and ZEKE-PES are clearly different (Fig. 2.22) [101]. The PI spectrum is a plot of ion current vs. wavelength of the probe laser. PI spectra show a simple rise of the curve at IE, while MATI and ZEKE yield a sharp peak at ionization threshold plus additional signals from lower vibrational ionization thresholds.

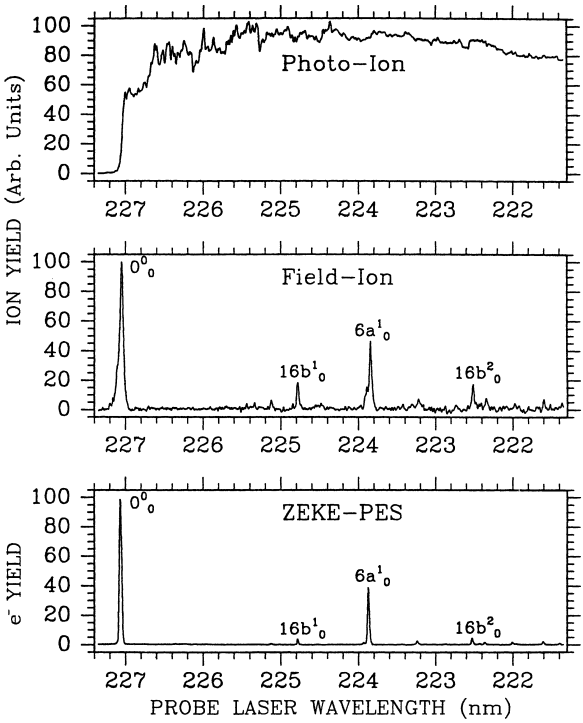

Fig. 2.22. Comparison of PI, MATI and ZEKE spectra of pyrazine. Reproduced from Ref. [101] with permission. © American Institute of Physics, 1991.

2.11 Determining the Appearance Energies

The techniques used for the determination of appearance energies are essentially identical to those described above for IEs. However, even when using the most accurately defined electron or photon energies, great care has to be taken when determining *AE*s because of the risk of overestimation due to kinetic shift. Provided that there is no reverse activation energy for the particular reaction, the *AE* value also delivers the sum of heats of formation of the dissociation products. If substantial KER is observed, the *AE* may still be used to determine the activation energy of the process.

2.11.1 Kinetic Shift

Fragment ion abundances observed by means of any mass spectrometer strongly depend on ion lifetimes within the ion source and on ion internal energy distributions, i.e., kinetic aspects play an important role for a mass spectrum's appearance.

As explained by QET the rate constant of an ion dissociation is a function of excess energy in the transition state of the respective reaction, and there is a need of substantial excess energy to make the rate constant exceed the critical 10^6 s^{-1} needed to dissociate during the residence times within the ion source. Therefore, appearance and activation energies are always in excess of the true values by the above amount. This phenomenon is known as *kinetic shift* (Fig. 2.23) [40,54]. Often, kinetic shifts are almost negligible (0.01–0.1 eV), but they can be as large as 2 eV, [40] e.g. an activation energy of 2.07 eV for $C_3H_6^{+\bullet} \rightarrow C_3H_5^+ + H^\bullet$ is accompanied by a kinetic shift of 0.19 eV [81]. As $k_{(E)}$ functions greatly differ between reactions and especially between homogeneous bond cleavages and rearrangement fragmentations, it is not an easy task to correct the experimental *AE*s by subtraction of E_{ex}. The influence of the kinetic shift can be minimized by increasing the ion source residence time and/or by increasing the detection sensitivity of the instrument.

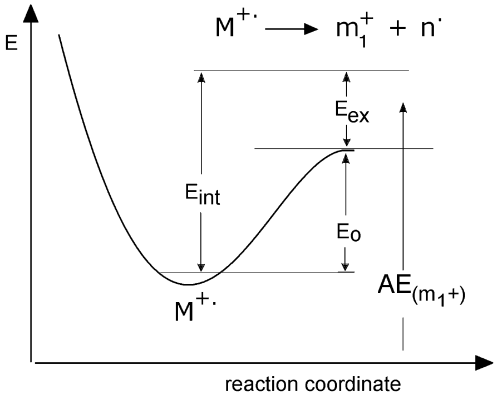

Fig. 2.23. Kinetic shift. The excess energy in the transition state affects *AE* measurements such that it always causes experimental values to be too high.

Note: The *kinetic shift* denotes the overestimation of *AE*s due to the contribution of excess energy in the transition state necessary to yield rate constants larger than 10^6 s^{-1}. The determination of IEs is not negatively affected by kinetic shift as kinetics is not involved in electron or photon ionization.

2.11.2 Breakdown Graphs

Employing the above techniques, one can examine the fragmentations of a molecular ion as a function of internal energy by constructing a so-called *breakdown graph*. This involves plotting the ion intensities of interest, i.e., those of a certain *m/z*, vs. electron energy or vs. ion internal energy if the *IE* has been subtracted before [106]. Typically, a molecular ion can access a considerable number of fragmentation pathways as soon as there are some 1–3 eV of internal energy available.

Breakdown graphs can be used to compare the energetic demands of those different fragmentation pathways. In addition, breakdown graphs help to correlate ion internal energy distributions derived from other methods such as photoelectron spectroscopy [107] with mass spectral data.

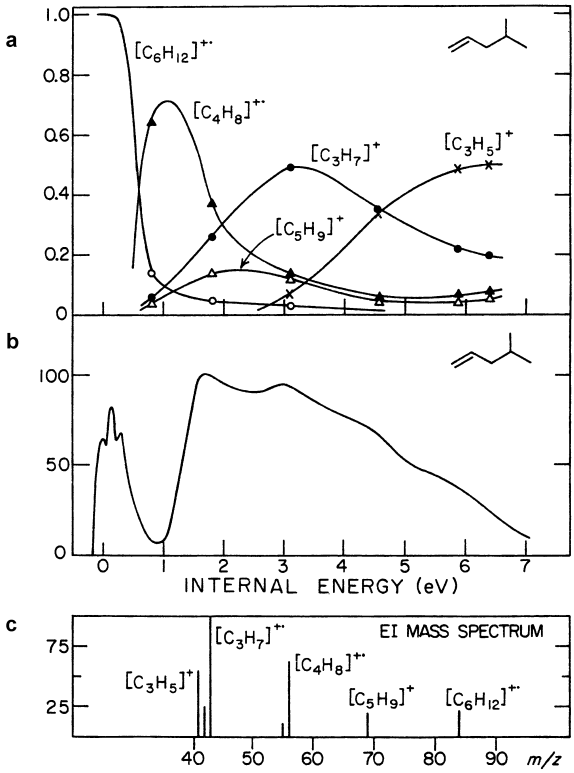

Fig. 2.24. 4-Methyl-1-pentene: (**a**) relationship of breakdown graph, (**b**) internal energy distribution from PES, and (**c**) mass spectrum. Reproduced from Ref. [108] by permission. © Wiley & Sons, 1982.

Example: For 4-methyl-1-pentene, the breakdown graph, the internal energy distribution from the PE spectrum, and the 70-eV EI mass spectrum are compared (Fig. 2.24) [108]. From the fragmentation threshold to about 2 eV of internal energy the breakdown graph is dominated by the $[C_4H_8]^{+\bullet}$ ion, *m/z* 56. In the range 2–4.5 eV the $[C_3H_7]^+$ ion, *m/z* 43, becomes most prominent. However, $[C_4H_8]^{+\bullet}$ only has 60% of the intensity of $[C_3H_7]^+$. It is obvious that the 0.5–1 eV energy region where the $[C_4H_8]^{+\bullet}$ fragment ion predominates corresponds to a region of the internal energy distribution that has a low ion population. This explains why $[C_3H_7]^+$ constitutes the base peak of the spectrum. Beyond 5 eV of internal energy, the $[C_3H_5]^+$ ion, *m/z* 41, becomes the most prominent fragment ion.

2.12 Gas Phase Basicity and Proton Affinity

Not all ionization methods rely on unimolecular conditions as strictly as EI does. Chemical ionization (CI, Chap. 7), for example, makes use of reactive collisions between ions generated from a reactant gas and the neutral analyte to achieve its ionization by some bimolecular process such as proton transfer. The question which reactant ion can protonate a given analyte can be answered from *gas phase basicity* (*GB*) or *proton affinity* (*PA*) data. Proton transfer, and thus the relative proton affinities of the reactants, also play an important role in many ion–neutral complex-mediated reactions (Chap. 6.12). In the last decade, *proton transfer reaction* (PTR) MS has emerged as a tool for analyzing *volatile organic compounds* (VOCs) in air. Therefore, PTR-MS is interesting for analytical work concerning environmental issues and in occupational health and safety (Chap. 7.3).

Here, we deal with proton affinity and gas phase basicity as thermodynamic quantities. Consider the following gas phase reaction of a (basic) molecule, B:

$$B_g + H_g^+ \rightarrow [BH]_g^+ \tag{2.34}$$

The tendency of B to accept a proton is then quantitatively described by

$$-\Delta G_r^0 = GB_{(B)} \quad \text{and} \quad -\Delta H_r^0 = PA_{(B)}\,, \tag{2.35}$$

i.e. the gas phase basicity $GB_{(B)}$ is defined as the negative free energy change for the proton transfer, $-\Delta G_r^0$, whereas the proton affinity $PA_{(B)}$ is the negative enthalpy change, $-\Delta H_r^0$, for the same reaction [109,110]. From the relation

$$\Delta G^0 = \Delta H^0 - T\,\Delta S^0 \tag{2.36}$$

we obtain the expression

$$PA_{(B)} = GB_{(B)} - T\,\Delta S^0 \tag{2.37}$$

with the entropy term $T\Delta S^0$ usually being relatively small (25–40 kJ mol^{-1}). Furthermore, in case of an equilibrium

$$[AH]^+ + B \rightleftharpoons A + [BH]^+ \tag{2.38}$$

with the equilibrium constant K_{eq} for which we have

$$K_{eq} = [BH^+]/[AH^+] \times [A]/[B] \tag{2.39}$$

the gas phase basicity is related to K_{eq} by [113,114]

$$GB_{(B)} = -\Delta G^0 = RT \ln K_{eq} \tag{2.40}$$

For the experimental determination of *GB*s and *PA*s refer to Chap. 9.18.3. Some representative *PA* and *GB* values are collected in Table 2.6.

Table 2.6. Selected proton affinities and gas phase basicities [23,109,113]

Molecule	$PA_{(B)}$ [kJ mol^{-1}]	$GB_{(B)}$ [kJ mol^{-1}]
H_2	424	396
CH_4	552	527
C_2H_6	601	558
H_2O	697	665
$H_2C{=}O$	718	685
$CH_3CH{=}CH_2$	751	718
C_6H_6 (benzene)	758	731
$(CH_3)_2C{=}CH_2$	820	784
$(CH_3)_2C{=}O$	823	790
$C_{14}H_{10}$ (phenanthrene)	831	802
C_4H_8O (tetrahydrofurane)	831	801
$C_2H_5OC_2H_5$	838	805
NH_3	854	818
CH_3NH_2	896	861
C_5H_5N (pyridine)	924	892
$(CH_3)_3N$	942	909

References

1. Porter, C.J.; Beynon, J.H.; Ast, T. The Modern Mass Spectrometer. A Complete Chemical Laboratory. *Org. Mass Spectrom.* **1981,** *16*, 101-114.
2. Schwarz, H. The Chemistry of Naked Molecules or the Mass Spectrometer As a Laboratory. *Chem. Unserer Zeit* **1991,** *25*, 268-278.
3. Kazakevich, Y. Citation Used by Permission. *http://hplc.chem.shu.edu/* **1996,** Seton Hall Univ., South Orange, NJ.
4. Cooks, R.G.; Beynon, J.H.; Caprioli, R.M. *Metastable Ions*; Elsevier: Amsterdam, 1973.
5. Levsen, K. *Fundamental Aspects of Organic Mass Spectrometry;* VCH: Weinheim, 1978.
6. Franklin, J.L. Energy Distributions in the Unimolecular Decomposition of Ions, in *Gas Phase Ion Chemistry*; Bowers, M.T. (ed.); Academic Press: New York, 1979; Vol. 1, Chap. 7, pp. 272-303.
7. Beynon, J.H.; Gilbert, J.R. Energetics and Mechanisms of Unimolecular Reactions of Positive Ions: Mass Spectrometric Methods, in *Gas Phase Ion Chemistry*; Bowers, M.T. (ed.); Academic Press: New York, 1979; Vol. 2, Chap. 13, pp. 153-179.
8. Vogel, P. The Study of Carbocations in the Gas Phase, in *Carbocation Chemistry*; Elsevier: Amsterdam, 1985; Chap. 2, pp. 61-84.
9. Holmes, J.L. Assigning Structures to Ions in the Gas Phase. *Org. Mass Spectrom.* **1985,** *20*, 169-183.
10. Lorquet, J.C. Basic Questions in MS. *Org. Mass Spectrom.* **1981,** *16*, 469-481.
11. Lorquet, J.C. Landmarks in the Theory of Mass Spectra. *Int. J. Mass Spectrom.* **2000,** *200*, 43-56.
12. Märk, T.D. Fundamental Aspects of Electron Impact Ionization. *Int. J. Mass Spectrom. Ion Phys.* **1982,** *45*, 125-145.
13. Märk, T.D. Electron Impact Ionization, in *Gaseous ion Chemistry and Mass Spectrometry*, Futrell, J.H. (ed.); Wiley: New York, 1986; pp. 61-93.
14. Wolkenstein, K.; Gross, J.H.; Oeser, T.; Schöler, H.F. Spectroscopic Characterization and Crystal Structure of the 1,2,3,4,5,6-Hexahydrophen-anthro-[1,10,9,8-*opqra*]Perylene. *Tetrahedron Lett.* **2002,** *43*, 1653-1655.

15. Schröder, E. *Massenspektrometrie – Begriffe und Definitionen*; Springer-Verlag: Heidelberg, 1991.
16. Harrison, A.G. Fundamentals of Gas Phase Ion Chemistry, in *Chemical Ionization Mass Spectrometry*, 2nd ed.; CRC Press: Boca Raton, 1992; Chap. 2, pp. 26.
17. De Wall, R.; Neuert, H. The Formation of Negative Ions From Electron Impact With Tungsten Hexafluoride. *Z. Naturforsch.,A.* **1977,** *32A*, 968-971.
18. Jones, E.G.; Harrison, A.G. Study of Penning Ionization Reactions Using a Single-Source Mass Spectrometer. *Int. J. Mass Spectrom. Ion Phys.* **1970,** *5*, 137-156.
19. Penning, F.M. Ionization by Metastable Atoms. *Naturwissenschaften* **1927,** *15*, 818.
20. Hornbeck, J.A.; Molnar, J.P. Mass-Spectrometric Studies of Molecular Ions in the Noble Gases. *Phys. Rev.* **1951,** *84*, 621-625.
21. Faubert, D.; Paul, G.J.C.; Giroux, J.; Betrand, M.J. Selective Fragmentation and Ionization of Organic Compounds Using an Energy-Tunable Rare-Gas Metastable Beam Source. *Int. J. Mass Spectrom. Ion Proc.* **1993,** *124*, 69-77.
22. Svec, H.J.; Junk, G.A. Electron-Impact Studies of Substituted Alkanes. *J. Am. Chem. Soc.* **1967,** *89*, 790-796.
23. NIST Chemistry Webbook. *http://webbook. nist.gov/* **2002**.
24. Honig, R.E. Ionization Potentials of Some Hydrocarbon Series. *J. Chem. Phys.* **1948,** *16*, 105-112.
25. Baldwin, M.; Kirkien-Konasiewicz, A.; Loudon, A.G.; Maccoll, A.; Smith, D. Localized or Delocalized Charges in Molecule-Ions? *Chem. Commun.* **1966,** 574.
26. McLafferty, F.W. Generalized Mechanism for Mass Spectral Reactions. *Chem. Commun.* **1966,** 78-80.
27. Wellington, C.A.; Khowaiter, S.H. Charge Distributions in Molecules and Ions: MINDO 3 Calculations. An Alternative of the Charge Localization Concept in Mass Spectrometry. *Tetrahedron* **1978,** *34*, 2183-2190.
28. Baldwin, M.A.; Welham, K.J. Charge Localization by Molecular Orbital Calculations. I. Urea and Thiourea. *Rapid. Commun. Mass Spectrom.* **1987,** *1*, 13-15.
29. Baldwin, M.A.; Welham, K.J. Charge Localization by Molecular Orbital Calculations. II. Formamide, Thioformamide and *N*-Methylated Analogs. *Org. Mass Spectrom.* **1988,** *23*, 425-428.
30. Weinkauf, R.; Lehrer, F.; Schlag, E.W.; Metsala, A. Investigation of Charge Localization and Charge Delocalization in Model Molecules by Multiphoton Ionization Photoelectron Spectroscopy and DFT Calculations. *Faraday Discussions* **2000,** *115*, 363-381.
31. Cone, C.; Dewar, M.J.S.; Landman, D. Gaseous Ions. 1. MINDO/3 Study of the Rearrangement of Benzyl Cation to Tropylium. *J. Am. Chem. Soc.* **1977,** *99*, 372-376.
32. Born, M.; Oppenheimer, J.R. Zur Quantentheorie Der Molekeln. *Annalen der Physik* **1927,** *84*, 457-484.
33. Seiler, R. Born-Oppenheimer Approximation. *International Journal of Quantum Chemistry* **1969,** *3*, 25-32.
34. Lipson, R.H. Ultraviolet and Visible Absorption Spectroscopy, in *Encyclopedia of Applied Spectroscopy*, Andrews, D.L. (ed.); Wiley-VCH: Berlin, 2009; Chap. 11, pp. 353-380.
35. Franck, J. Elementary Processes of Photochemical Reactions. *Trans. Faraday Soc.* **1925,** *21*, 536-542.
36. Condon, E.U. Theory of Intensity Distribution in Band Systems. *Phys. Rev.* **1926,** *28*, 1182-1201.
37. Dunn, G.H. Franck-Condon Factors for the Ionization of H_2 and D_2. *J. Chem. Phys.* **1966,** *44*, 2592-2594.
38. Märk, T.D. Fundamental Aspects of Electron Impact Ionization. *Int. J. Mass Spectrom. Ion Phys.* **1982,** *45*, 125-145.
39. Märk, T.D. Electron Impact Ionization, in *Gaseous ion Chemistry and MS*, Futrell, J.H. (ed.); Wiley: New York, 1986; pp. 61-93.
40. McLafferty, F.W.; Wachs, T.; Lifshitz, C.; Innorta, G.; Irving, P. Substituent Effects in Unimolecular Ion Decompositions. XV. Mechanistic Interpretations and the Quasi-Equilibrium Theory. *J. Am. Chem. Soc.* **1970,** *92*, 6867-6880.
41. Egger, K.W.; Cocks, A.T. Homopolar- and Heteropolar Bond Dissociation Energies and Heats of Formation of Radicals and Ions in the Gas Phase. I. Data on Organic Molecules. *Helv. Chim. Acta* **1973,** *56*, 1516-1536.

42. Lossing, F.P.; Semeluk, G.P. Free Radicals by Mass Spectrometry. XLII. Ionization Potentials and Ionic Heats of Formation for C_1-C_4 Alkyl Radicals. *Can. J. Chem.* **1970,** *48*, 955-965.
43. Lossing, F.P.; Holmes, J.L. Stabilization Energy and Ion Size in Carbocations in the Gas Phase. *J. Am. Chem. Soc.* **1984,** *106*, 6917-6920.
44. Cox, J.D.; Pilcher, G. *Thermochemistry of Organic and Organometallic Compounds*; Academic Press: London, 1970.
45. Chatham, H.; Hils, D.; Robertson, R.; Gallagher, A. Total and Partial Electron Collisional Ionization Cross Sections for Methane, Ethane, Silane, and Disilane. *J. Chem. Phys.* **1984,** *81*, 1770-1777.
46. Wahrhaftig, A.L. Ion Dissociations in the Mass Spectrometer, in *Advances in Mass Spectrometry*, Waldron, J.D (ed.); Pergamon: Oxford, 1959; pp. 274-286.
47. Wahrhaftig, A.L. Unimolecular Dissociations of Gaseous Ions, in *Gaseous ion Chemistry and MS*, Futrell, J.H. (ed.); Wiley: New York, 1986; pp. 7-24.
48. Rosenstock, H.M.; Krauss, M. Quasi-Equilibrium Theory of Mass Spectra, in *Mass Spectrometry of Organic Ions*; McLafferty, F.W. (ed.); Academic Press: London, 1963; pp. 1-64.
49. Bohme, D.K.; Mackay, G.I. Bridging the Gap Between the Gas Phase and Solution: Transition in the Kinetics of Nucleophilic Displacement Reactions. *J. Am. Chem. Soc.* **1981,** *103*, 978-979.
50. Speranza, M. Gas Phase Ion Chemistry Versus Solution Chemistry. *Int. J. Mass Spectrom. Ion Proc.* **1992,** *118/119*, 395-447.
51. Rosenstock, H.M.; Wallenstein, M.B.; Wahrhaftig, A.L.; Eyring, H. Absolute Rate Theory for Isolated Systems and the Mass Spectra of Polyatomic Molecules. *Proc. Natl. Acad. Sci. U.S.A.* **1952,** *38*, 667-678.
52. McAdoo, D.J.; Bente, P.F.I.; Gross, M.L.; McLafferty, F.W. Metastable Ion Characteristics. XXIII. Internal Energy of Product Ions Formed in Massspectral Reactions. *Org. Mass Spectrom.* **1974,** *9*, 525-535.
53. Meier, K.; Seibl, J. Measurement of Ion Residence Times in a Commercial Electron Impact Ion Source. *Int. J. Mass Spectrom. Ion Phys.* **1974,** *14*, 99-106.
54. Chupka, W.A. Effect of Unimolecular Decay Kinetics on the Interpretation of Appearance Potentials. *J. Chem. Phys.* **1959,** *30*, 191-211.
55. Holmes, J.L.; Terlouw, J.K. The Scope of Metastable Peak Shape Observations. *Org. Mass Spectrom.* **1980,** *15*, 383-396.
56. Williams, D.H. A Transition State Probe. *Acc. Chem. Res.* **1977,** *10*, 280-286.
57. Williams, D.H.; Hvistendahl, G. Kinetic Energy Release in Relation to Symmetry-Forbidden Reactions. *J. Am. Chem. Soc.* **1974,** *96*, 6753-6755.
58. Williams, D.H.; Hvistendahl, G. Kinetic Energy Release As a Mechanistic Probe. The Role of Orbital Symmetry. *J. Am. Chem. Soc.* **1974,** *96*, 6755-6757.
59. Hvistendahl, G.; Williams, D.H. Partitioning of Reverse Activation Energy Between Kinetic and Internal Energy in Reactions of Simple Organic Ions. *J. Chem. Soc.,Perkin Trans. 2* **1975,** 881-885.
60. Hvistendahl, G.; Uggerud, E. Secondary Isotope Effect on Kinetic Energy Release and Reaction Symmetry. *Org. Mass Spectrom.* **1985,** *20*, 541-542.
61. Kim, K.C.; Beynon, J.H.; Cooks, R.G. Energy Partitioning by Mass Spectrometry. Chloroalkanes and Chloroalkenes. *J. Chem. Phys.* **1974,** *61*, 1305-1314.
62. Haney, M.A.; Franklin, J.L. Correlation of Excess Energies of Electron Impact Dissociations With the Translational Energies of the Products. *J. Chem. Phys.* **1968,** *48*, 4093-4097.
63. Cooks, R.G.; Williams, D.H. The Relative Rates of Fragmentation of Benzoyl Ions Generated Upon Electron Impact From Different Precursors. *Chem. Commun.* **1968,** 627-629.
64. Lin, Y.N.; Rabinovitch, B.S. Degrees of Freedom Effect and Internal Energy Partitioning Upon Ion Decomposition. *J. Phys. Chem.* **1970,** *74*, 1769-1775.
65. Bente III., P.F.; McLafferty, F.W.; McAdoo, D.J.; Lifshitz, C. Internal Energy of Product Ions Formed in Mass Spectral Reactions. The Degrees of Freedom Effect. *J. Phys. Chem.* **1975,** *79*, 713-721.
66. Todd, J.F.J. Recommendations for Nomenclature and Symbolism for Mass Spectroscopy Including an Appendix of Terms Used in Vacuum Technology. *Int. J. Mass Spectrom. Ion. Proc.* **1995,** *142*, 211-240.
67. Robinson, P.J.; Holbrook, K.A. Unimolecular Reactions, in *Unimolecular*

Re-actions, Wiley: London, 1972; Chap. 9.

68. Ingemann, S.; Hammerum, S.; Derrick, P.J.; Fokkens, R.H.; Nibbering, N.M.M. Energy-Dependent Reversal of Secondary Isotope Effects on Simple Cleavage Reactions: Tertiary Amine Radical Cations With Deuterium at Remote Positions. *Org. Mass Spectrom.* **1989,** *24*, 885-889.
69. Lowry, T.H.; Schueller Richardson, K. Isotope Effects, in *Mechanism and Theory in Organic Chemistry*; Harper and Row: New York, 1976; Chap. 1.7.
70. Stringer, M.B.; Underwood, D.J.; Bowie, J.H.; Allison, C.E.; Donchi, K.F.; Derrick, P.J. Is the McLafferty Rearrangement of Ketones Concerted or Stepwise? The Application of Kinetic Isotope Effects. *Org. Mass Spectrom.* **1992,** *27*, 270-276.
71. Derrick, P.J. Isotope Effects in Fragmentation. *Mass Spectrom. Rev.* **1983,** *2*, 285-298.
72. Hvistendahl, G.; Uggerud, E. Deuterium Isotope Effects and Mechanism of the Gas-Phase Reaction $[C_3H_7]^+ \rightarrow [C_3H_5]^+ + H_2$. *Org. Mass Spectrom.* **1986,** *21*, 347-350.
73. Howe, I.; McLafferty, F.W. Unimolecular Decomposition of Toluene and Cycloheptatriene Molecular Ions. Variation of the Degree of Scrambling and Isotope Effect With Internal Energy. *J. Am. Chem. Soc.* **1971,** *93*, 99-105.
74. Bertrand, M.; Beynon, J.H.; Cooks, R.G. Isotope Effects Upon Hydrogen Atom Loss From Molecular Ions. *Org. Mass Spectrom.* **1973,** *7*, 193-201.
75. Lau, A.Y.K.; Solka, B.H.; Harrison, A.G. Isotope Effects and H/D Scrambling in the Fragmentation of Labeled Propenes. *Org. Mass Spectrom.* **1974,** *9*, 555-557.
76. Benoit, F.M.; Harrison, A.G. Hydrogen Migrations in Mass Spectrometry. I. The Loss of Olefin From Phenyl-*n*-Propyl Ether Following Electron Impact Ionization and Chemical Ionization. *Org. Mass Spectrom.* **1976,** *11*, 599-608.
77. Veith, H.J.; Gross, J.H. Alkene Loss From Metastable Methyleneimmonium Ions: Unusual Inverse Secondary Isotope Effect in Ion–Neutral Complex Intermediate Fragmentations. *Org. Mass Spectrom.* **1991,** *26*, 1097-1105.
78. Ingemann, S.; Kluft, E.; Nibbering, N.M.M.; Allison, C.E.; Derrick, P.J.; Hammerum, S. Time-Dependence of the Isotope Effects in the Unimolecular Dissociation of Tertiary Amine Molecular Ions. *Org. Mass Spectrom.* **1991,** *26*, 875-881.
79. Nacson, S.; Harrison, A.G. Dependence of Secondary Hydrogen/Deuterium Isotope Effects on Internal Energy. *Org. Mass Spectrom.* **1985,** *20*, 429-430.
80. Ingemann, S.; Hammerum, S.; Derrick, P.J. Secondary Hydrogen Isotope Effects on Simple Cleavage Reactions in the Gas Phase: The α-Cleavage of Tertiary Amine Cation Radicals. *J. Am. Chem. Soc.* **1988,** *110*, 3869-3873.
81. Rosenstock, H.M. The Measurement of Ionization and Appearance Potentials. *Int. J. Mass Spectrom. Ion Phys.* **1976,** *20*, 139-190.
82. Urban, B.; Bondybey, V.E. Multiphoton Photoelectron Spectroscopy: Watching Molecules Dissociate. *Phys. Chem. Chem. Phys.* **2001,** *3*, 1942-1944.
83. Nicholson, A.J.C. Measurement of Ionization Potentials by Electron Impact. *J. Chem. Phys.* **1958,** *29*, 1312-1318.
84. Barfield, A.F.; Wahrhaftig, A.L. Determination of Appearance Potentials by the Critical Slope Method. *J. Chem. Phys.* **1964,** *41*, 2947-2948.
85. Levin, R.D.; Lias, S.G. Ionization Potential and Appearance Potential Measurements, 1971-1981. *National Standard Reference Data Series* **1982,** *71*, 634 pp.
86. Harris, F.M.; Beynon, J.H. Photodissociation in Beams: Organic Ions, in *Gas Phase Ion Chemistry – Ions and Light*; Bowers, M.T. (ed.); Academic Press: New York, 1985; Vol. 3, Chap. 19, pp. 99-128.
87. Dunbar, R.C. Ion Photodissociation, in *Gas Phase Ion Chemistry*; Bowers, M.T. (ed.); Academic Press: New York, 1979; Vol. 2, Chap. 14, pp. 181-220.
88. Maeda, K.; Semeluk, G.P.; Lossing, F.P. A Two-Stage Double-Hemispherical Electron Energy Selector. *Int. J. Mass Spectrom. Ion Phys.* **1968,** *1*, 395-407.
89. Traeger, J.C.; McLoughlin, R.G. A Photoionization Study of the Energetics of the $C_7H_7^+$ Ion Formed from C_7H_8 Precursors. *Int. J. Mass Spectrom. Ion Phys.* **1978,** *27*, 319-333.
90. Boesl, U. Laser MS for Environmental and Industrial Chemical Trace Analysis. *J. Mass Spectrom.* **2000,** *35*, 289-304.

91. Wendt, K.D.A. The New Generation of Resonant Laser Ionization Mass Spectrometers: Becoming Competitive for Selective Atomic Ultra-Trace Determination? *Eur. J. Mass Spectrom.* **2002,** *8*, 273-285.
92. Matsumoto, J.; Misawa, K.; Ishiuchi, S.I.; Suzuki, T.; Hayashi, S.I.; Fujii, M. On-Site and Real-Time Mass Spectrometer Utilizing the Resonance-Enhanced Multiphoton Ionization Technique. *Shinku* **2007,** *50*, 241-245.
93. Thanner, R.; Oser, H.; Grotheer, H.-H. Time-Resolved Monitoring of Aromatic Compounds in an Experimental Incinerator Using an Improved Jet-Resonance-Enhanced Multi-Photon Ionization System Jet-REMPI. *Eur. Mass Spectrom.* **1998,** *4*, 215-222.
94. Zenobi, R.; Zhan, Q.; Voumard, P. Multiphoton Ionization Spectroscopy in Surface Analysis and Laser Desorption MS. *Mikrochimica Acta* **1996,** *124*, 273-281.
95. Weickhardt, C.; Grun, C.; Grotemeyer, J. Fundamentals and Features of Analytical Laser MS With Ultrashort Laser Pulses. *Eur. Mass Spectrom.* **1998,** *4*, 239-244.
96. Turner, D.W.; Al Jobory, M.I. Determination of Ionization Potentials by Photoelectron Energy Measurement. *J. Chem. Phys.* **1962,** *37*, 3007-3008.
97. Müller-Dethlefs, K.; Sander, M.; Schlag, E.W. Two-Color Photoionization Resonance Spectroscopy of Nitric Oxide: Complete Separation of Rotational Levels of Nitrosyl Ion at the Ionization Threshold. *Chem. Phys. Lett.* **1984,** *112*, 291-294.
98. Müller-Dethlefs, K.; Sander, M.; Schlag, E.W. A Novel Method Capable of Resolving Rotational Ionic States by the Detection of Threshold Photoelectrons With a Resolution of 1.2 Cm^{-1}. *Z. Naturforsch.* **1984,** *39a*, 1089-1091.
99. Schlag, E.W. *ZEKE Spectroscopy*; Cambridge Univ. Press: Cambridge, 1998.
100. Edqvist, O.; Lindholm, E.; Selin, L.E.; Åsbrink, L. Photoelectron Spectrum of Molecular Oxygen. *Phys. Scr.* **1970,** *1*, 25-30.
101. Zhu, L.; Johnson, P. Mass Analyzed Threshold Ionization Spectroscopy. *J. Chem. Phys.* **1991,** *94*, 5769-5771.
102. Weickhardt, C.; Moritz, F.; Grotemeyer, J. Time-of-Flight MS: State-of-the-Art in Chemical Analysis and Molecular Science. *Mass Spectrom. Rev.* **1997,** *15*, 139-162.
103. Gunzer, F.; Grotemeyer, J. New Features in the Mass Analyzed Threshold Ionization (MATI) Spectra of Alkyl Benzenes. *Phys. Chem. Chem. Phys.* **2002,** *4*, 5966-5972.
104. Peng, X.; Kong, W. Zero Energy Kinetic Electron and Mass-Analyzed Threshold Ionization Spectroscopy of $Na\times(NH_3)_n$ (n=1,2,and 4) Complexes. *J. Chem. Phys.* **2002,** *117*, 9306-9315.
105. Haines, S.R.; Dessent, C.E.H.; Müller-Dethlefs, K. Mass Analyzed Threshold Ionization of Phenol×CO: Intermolecular Binding Energies of a Hydrogen-Bonded Complex. *J. Chem. Phys.* **1999,** *111*, 1947-1954.
106. Lavanchy, A.; Houriet, R.; Gäumann, T. The Mass Spectrometric Fragmentation of *N*-Heptane. *Org. Mass Spectrom.* **1978,** *13*, 410-416.
107. Meisels, G.G.; Chen, C.T.; Giessner, B.G.; Emmel, R.H. Energy-Deposition Functions in Mass Spectrometry. *J. Chem. Phys.* **1972,** *56*, 793-800.
108. Herman, J.A.; Li, Y.-H.; Harrison, A.G. Energy Dependence of the Fragmentation of Some Isomeric $C_6H_{12}^{+\cdot}$ Ions. *Org. Mass Spectrom.* **1982,** *17*, 143-150.
109. Lias, S.G.; Liebman, J.F.; Levin, R.D. Evaluated Gas Phase Basicities and Proton Affinities of Molecules; Heats of Formation of Protonated Molecules. *J. Phys. Chem. Ref. Data* **1984,** *13*, 695-808.
110. Harrison, A.G. The Gas-Phase Basicities and Proton Affinities of Amino Acids and Peptides. *Mass Spectrom. Rev.* **1997,** *16*, 201-217.
111. Kukol, A.; Strehle, F.; Thielking, G.; Grützmacher, H.-F. Methyl Group Effect on the Proton Affinity of Methylated Acetophenones Studied by Two MS Techniques. *Org. Mass Spectrom.* **1993,** *28*, 1107-1110.
112. McMahon, T.B. Thermochemical Ladders: Scaling the Ramparts of Gaseous Ion Energetics. *Int. J. Mass Spectrom.* **2000,** *200*, 187-199.
113. Lias, S.G.; Bartmess, J.E.; Liebman, J.F.; Holmes, J.L.; Levin, R.D.; Mallard, W.G. Gas-Phase Ion and Neutral Thermochemistry. *J. Phys. Chem. Ref. Data* **1988,** *17, Supplement 1*, 861 pp.

http://www.springer.com/978-3-642-10709-2

Mass Spectrometry
A Textbook
Gross, J.H.
2011, XXIV, 753 p., Hardcover
ISBN: 978-3-642-10709-2